

## INFORMATION TO USERS

The most advanced technology has been used to photograph and reproduce this manuscript from the microfilm master. UMI films the text directly from the original or copy submitted. Thus, some thesis and dissertation copies are in typewriter face, while others may be from any type of computer printer.

The quality of this reproduction is dependent upon the quality of the copy submitted. Broken or indistinct print, colored or poor quality illustrations and photographs, print bleedthrough, substandard margins, and improper alignment can adversely affect reproduction.

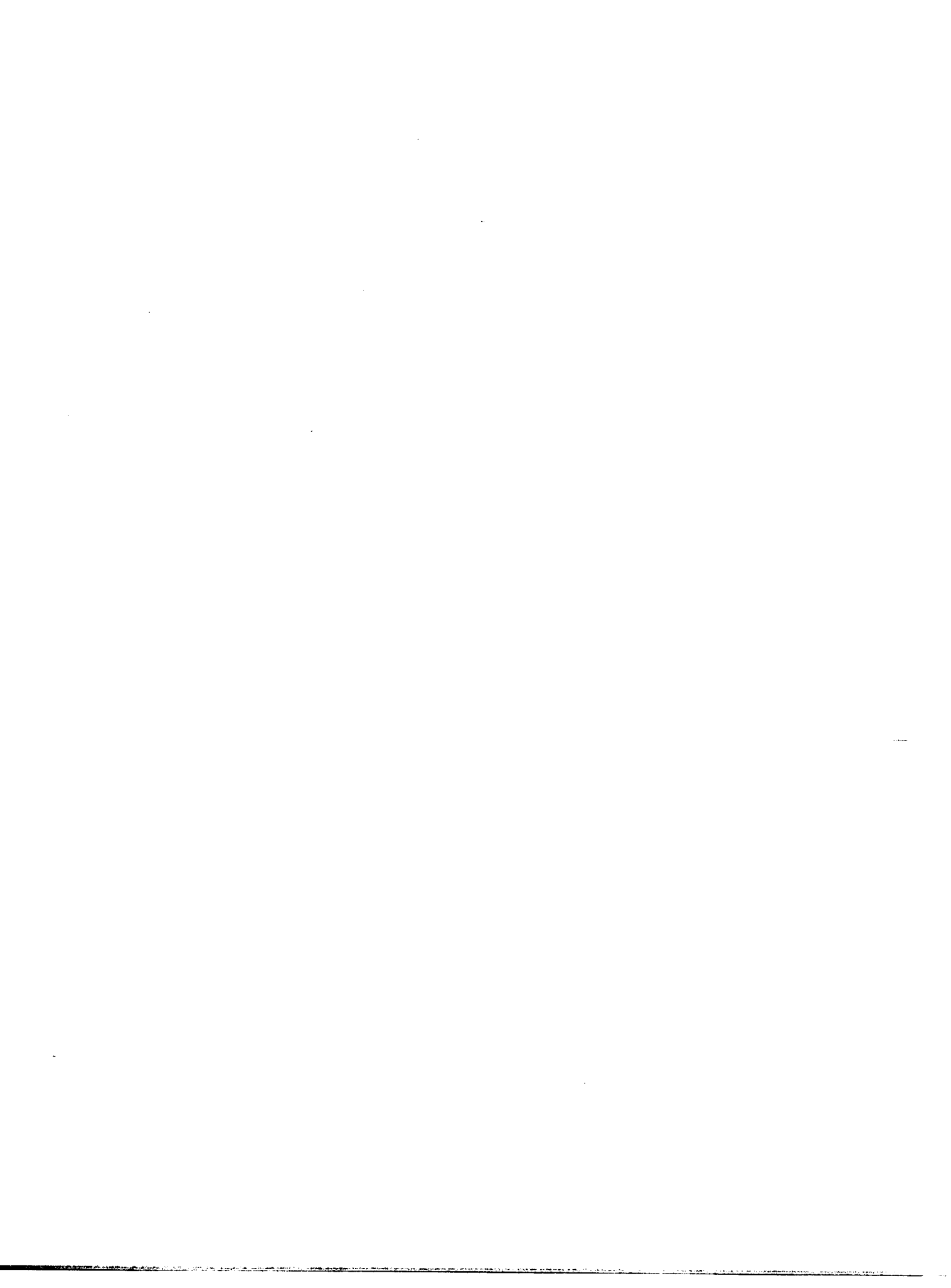
In the unlikely event that the author did not send UMI a complete manuscript and there are missing pages, these will be noted. Also, if unauthorized copyright material had to be removed, a note will indicate the deletion.

Oversize materials (e.g., maps, drawings, charts) are reproduced by sectioning the original, beginning at the upper left-hand corner and continuing from left to right in equal sections with small overlaps. Each original is also photographed in one exposure and is included in reduced form at the back of the book. These are also available as one exposure on a standard 35mm slide or as a 17" x 23" black and white photographic print for an additional charge.

Photographs included in the original manuscript have been reproduced xerographically in this copy. Higher quality 6" x 9" black and white photographic prints are available for any photographs or illustrations appearing in this copy for an additional charge. Contact UMI directly to order.

# U·M·I

University Microfilms International  
A Bell & Howell Information Company  
300 North Zeeb Road, Ann Arbor, MI 48106-1346 USA  
313/761-4700 800/521-0600



Order Number 1335052

**Scanning tunneling microscopy of layered-structure  
semiconductors**

Henson, Tammy Deanne, M.S.

The University of Arizona, 1988

**U·M·I**

300 N. Zeeb Rd.  
Ann Arbor, MI 48106



SCANNING TUNNELING MICROSCOPY  
OF LAYERED-STRUCTURE SEMICONDUCTORS

by

Tammy Deanne Henson



A Thesis Submitted to the Faculty of the  
COMMITTEE ON OPTICAL SCIENCES (GRADUATE)  
In Partial Fulfillment of the Requirements  
For the Degree of  
MASTER OF SCIENCE  
In the Graduate College  
THE UNIVERSITY OF ARIZONA

1 9 8 8

## STATEMENT BY AUTHOR

This thesis has been submitted in partial fulfillment of requirements for an advanced degree at the University of Arizona and is deposited in the University Library to be made available to borrower's under the rules of the Library.

Brief quotations from this thesis are allowable without special permission, provided that accurate acknowledgment of source is made. Requests for permission for extended quotation from or reproduction of this manuscript in whole or in part may be granted by the head of the major department or the Dean of the Graduate College when in his or her judgment the proposed use of the material is in the interests of scholarship. In all other instances, however, permission must be obtained from the author.

SIGNED: Sammy Henson

## APPROVAL BY THESIS DIRECTOR

This thesis has been approved on the date shown below:

D. Sarid

Dror Sarid  
Professor of Optical Sciences

7-20-88  
Date

### Acknowledgements

I would like to thank my advisor, Dror Sarid, who introduced me to the world of scanning tunneling microscopy and provided me with the topic of this thesis. I especially appreciate his help in the interpretation of the data and the constant source of encouragement he provided.

I thank Doug Smith who provided the scanning tunneling microscope (STM) head and electronic schematics. Without his help, the STM system would not have become operational as quickly as it did. I am grateful to Steve Bell, Ray Hawksley and John Doherty for all of the electronic support they provided for the STM system. Their help and support were invaluable for the completion and subsequent modifications of the STM system electronics. I thank Yaw-Huei Chen and Pishien Liu for the software support they provided that allowed me to transfer my images and spectroscopic curves to a personal computer where further processing of my data could take place. Without their help, I would not have been able to present many of the figures in this thesis. I thank Kevin Johnson who built the tip etching circuit, which provided many high quality tips and allowed me to obtain atomic resolution images on a number of different materials.

I am grateful to Mark Voelker and David Perry who showed me how to etch the tungsten tips and demonstrated basic operation of the STM system to me. With their help, I was able to obtain my first STM image just one week after the STM system became operational.

I thank Claude Sandroff for providing me with the methods to fabricate the semiconductor clusters used in this thesis, and Neil Armstrong who provided all the bulk semiconductor samples studied here and helped me to understand the chemistry of these structures.

Brian McGinnis, Merritt Deeter, Doug Iams, and Sam Howells, who are all members of Dror's group, acted as sounding boards for many scientific and personal matters. I appreciate their friendship and the support they gave me. I thank Doug for often helping to debug the STM system, and I am indebted to Brian for always seeming to have the answers to all my questions on a wide variety of subjects.

Finally, I thank my husband Bill, whose love and encouragement have seen me through graduate school, and my Lord Jesus Christ to whom goes all glory and praise.

## TABLE OF CONTENTS

	Page
LIST OF ILLUSTRATIONS .....	6
LIST OF TABLES .....	8
ABSTRACT .....	9
1. INTRODUCTION .....	10
Discovery .....	16
Theory .....	17
STM Applications .....	20
Organization of the Thesis .....	21
2. OUR STM SYSTEM .....	23
Image Processing .....	26
Vibration Isolation .....	28
Tip Preparation .....	29
3. BULK LAYERED-STRUCTURE SEMICONDUCTORS .....	31
Images .....	32
Density of States Measurement .....	40
Results and Conclusions .....	47
4. SEMICONDUCTOR CLUSTERS .....	48
Image of an Isolated Cluster on Graphite .....	49
MoS <sub>2</sub> Clusters on Graphite .....	51
Results and Conclusions .....	55

TABLE OF CONTENTS-Continued

5. FUTURE STM RESEARCH .....	60
Quantum Confinement of Charge Carriers in Semiconductor Clusters .	60
Improvements in Cluster Imaging .....	60
STM System Improvements .....	61
Summary .....	62
REFERENCES .....	63

## LIST OF ILLUSTRATIONS

Figure	Page
1.1 The constant current mode of operation for the STM .....	12
1.2 The constant height mode of operation for the STM .....	13
1.3 Feedback network for the constant height mode of operation .....	14
2.1 Schematic drawing of the STM system used in this study .....	24
2.2 Grey scale image of the surface of graphite .....	25
2.3 Grey scale image of a cluster on the surface of graphite (a) unfiltered and (b) filtered .....	27
3.1 Atomically resolved grey scale image of MoS <sub>2</sub> obtained with a positive sample bias .....	34
3.2 Atomically resolved grey scale image of WSe <sub>2</sub> obtained with a positive sample bias .....	35
3.3 Atomically resolved grey scale image of SnS <sub>2</sub> obtained with a positive sample bias .....	36
3.4 Atomically resolved grey scale image of MoS <sub>2</sub> obtained with a negative sample bias .....	37
3.5 Atomically resolved grey scale image of WSe <sub>2</sub> obtained with a negative sample bias .....	38
3.6 Atomically resolved grey scale image of SnS <sub>2</sub> obtained with a negative sample bias .....	39
3.7 Plots of (a) tunneling current (I) and (b) d(lnI)/d(lnV) as a function of bias voltage (V) for MoS <sub>2</sub> .....	44
3.8 Plots of (a) tunneling current (I) and (b) d(lnI)/d(lnV) as a function of bias voltage (V) for WSe <sub>2</sub> .....	45
3.9 Plots of (a) tunneling current (I) and (b) d(lnI)/d(lnV) as a function of bias voltage (V) for SnS <sub>2</sub> .....	46

LIST OF ILLUSTRATIONS-Continued

4.1	Predicted structure of layered $\text{PbI}_2$ and $\text{BiI}_3$ semiconductor clusters . . . .	50
4.2	Grey scale image of a cluster on the surface of graphite . . . . .	52
4.3	Three dimensional presentations of $\text{MoS}_2$ clusters on the surface of graphite . . . . .	56
4.4	Three dimensional presentations of $\text{MoS}_2$ clusters on the surface of graphite . . . . .	57
4.5	Grey scale image of $\text{MoS}_2$ island on the surface of graphite . . . . .	58
4.6	Grey scale image of atomically resolved $\text{MoS}_2$ island on the surface of graphite . . . . .	59

## LIST OF TABLES

Table	Page
1.1 Advantages and disadvantages of STM modes of operation . . . . .	15
3.1 Lattice parameters and energy gaps of bulk layered-structure semiconductors . . . . .	33
4.1 Lattice spacings observed on MoS <sub>2</sub> clusters . . . . .	54

## ABSTRACT

Semiconductors are characterized by atomic resolution imaging and density of states measurements (DOS) obtained through the use of a scanning tunneling microscope (STM). The DOS of the conduction and valence bands can be measured separately with a STM as opposed to an optical measurement which measures only the joint DOS. Layered-structure semiconductors are characterized both in the bulk form and in the isolated cluster form.

Images of three bulk layered-structure semiconductors,  $\text{MoS}_2$ ,  $\text{WSe}_2$ , and  $\text{SnS}_2$ , were obtained with both positive and negative sample-to-tip bias voltages. Curves of tunneling current as a function of bias voltage were measured, from which the DOS of the valence and conduction bands can be inferred.

We obtained an atomically resolved image of an isolated fragment of a semiconductor cluster which was deposited on a graphite surface from a colloidal suspension of  $\text{BiI}_3$ . Also imaged were clusters of  $\text{MoS}_2$  layered-structure semiconductors.

## CHAPTER 1

### INTRODUCTION

When the scanning tunneling microscope (STM) was invented in 1982 by Binnig and Rohrer (1982), a whole new atomic scale world was uncovered and atomic measuring capabilities were revolutionized. Since then, the STM has become an indispensable tool for studying the surface of materials by obtaining images of individual atoms in real space and measuring the density of states of the conduction and valence bands as well as those of surface states.

This thesis describes the characterization of layered-structure semiconductors by atomic resolution imaging and density of states measurements made with a STM. By studying layered-structure semiconductors in the bulk and in isolated cluster form, one can gain insight into how these clusters grow into the bulk form and how the bandgap and lattice parameters of a material change as a function of cluster size. By understanding the size-dependent properties of a material, one can learn how the linear optical response changes as a function of the size of a cluster.

The basic structure of a STM consists of a very sharp tungsten tip, having a single atom at the end, that is brought to within a few angstroms from the surface of a sample. The surface and the tip are close enough such that on the application of a bias voltage their electron clouds overlap, and a current tunnels between them. The tunneling current has the unique property that it is exponentially dependent on the tip-to-surface separation.

There are basically two modes of operation with a STM. The first mode, called the constant current mode, is demonstrated in Fig. 1.1 (Hansma and Tersoff 1987). In this mode, the tip is brought close to the surface until a tunneling current is detected. The tip is then raster scanned across the surface while the tunneling current is monitored. To keep the tunneling current constant a feedback network changes the height of the tip,  $z$ , such that the tip follows the terrain of the surface. Images of the topography of the surface are obtained using the  $x$ , and  $y$  raster scan and the  $z$  displacement of the tip. The second mode of operation, called the constant height mode, is demonstrated in Fig. 1.2 (Hansma and Tersoff 1987). In this mode, the feedback network takes the difference between the tunneling current and a set current value and passes it through a low pass filter whose bandpass is much narrower than the scan frequency. The output from the low pass filter is then sent to the  $z$  axis of the piezo tube, and the tip position is corrected in order to maintain a constant average height above the surface (See Fig. 1.3). One measures the change in the tunneling current as the tip is raster scanned across the surface. Images are obtained using the  $x$ , and  $y$  raster scan and the natural log of the tunneling current for the  $z$  value. The advantages and disadvantages of each mode of operation are listed in Table 1.1.

There are many methods for obtaining an image from the STM data. One common way of forming an image is to use a two dimensional line graph where a fraction of the  $z$  value is added to the  $y$  value which is plotted versus  $x$ , yielding a three dimensional representation of the surface. A second method is to produce a grey scale image where the  $x$ , and  $y$  of the image is plotted versus  $z$  which is an intensity or grey scale value. A third method, similar to the grey scale image, is to assign certain  $z$  values to different colors resulting in a false color image of

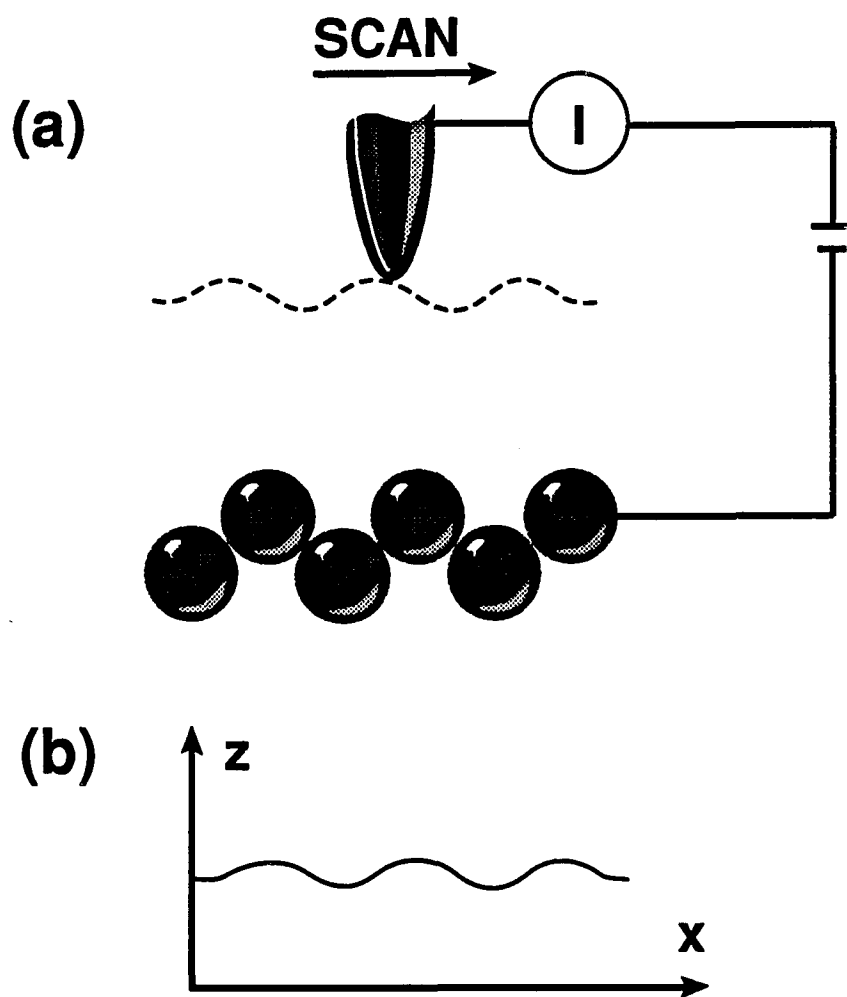


Figure 1.1 The constant current mode of operation for the STM, a) schematic representation and b) one single line scan. Note placing a number of line scans together creates the STM image.

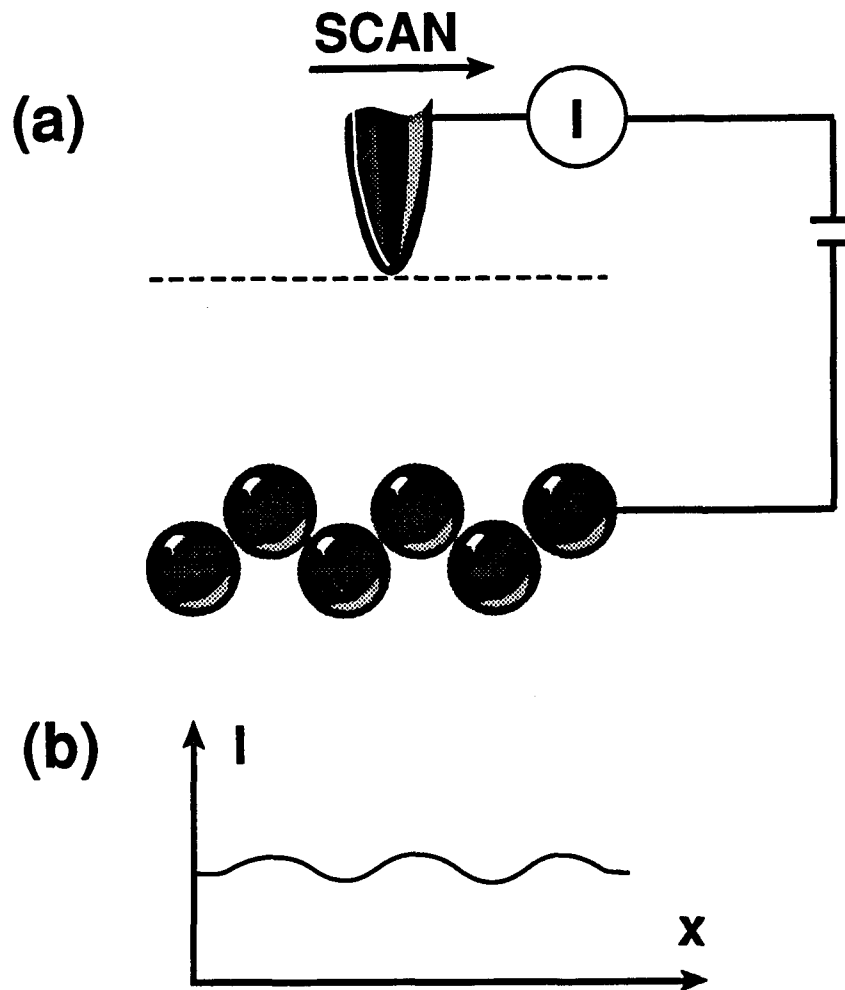


Figure 1.2 The constant height mode of operation for the STM, a) schematic representation and b) one single line scan. Note placing a number of line scans together creates the STM image.

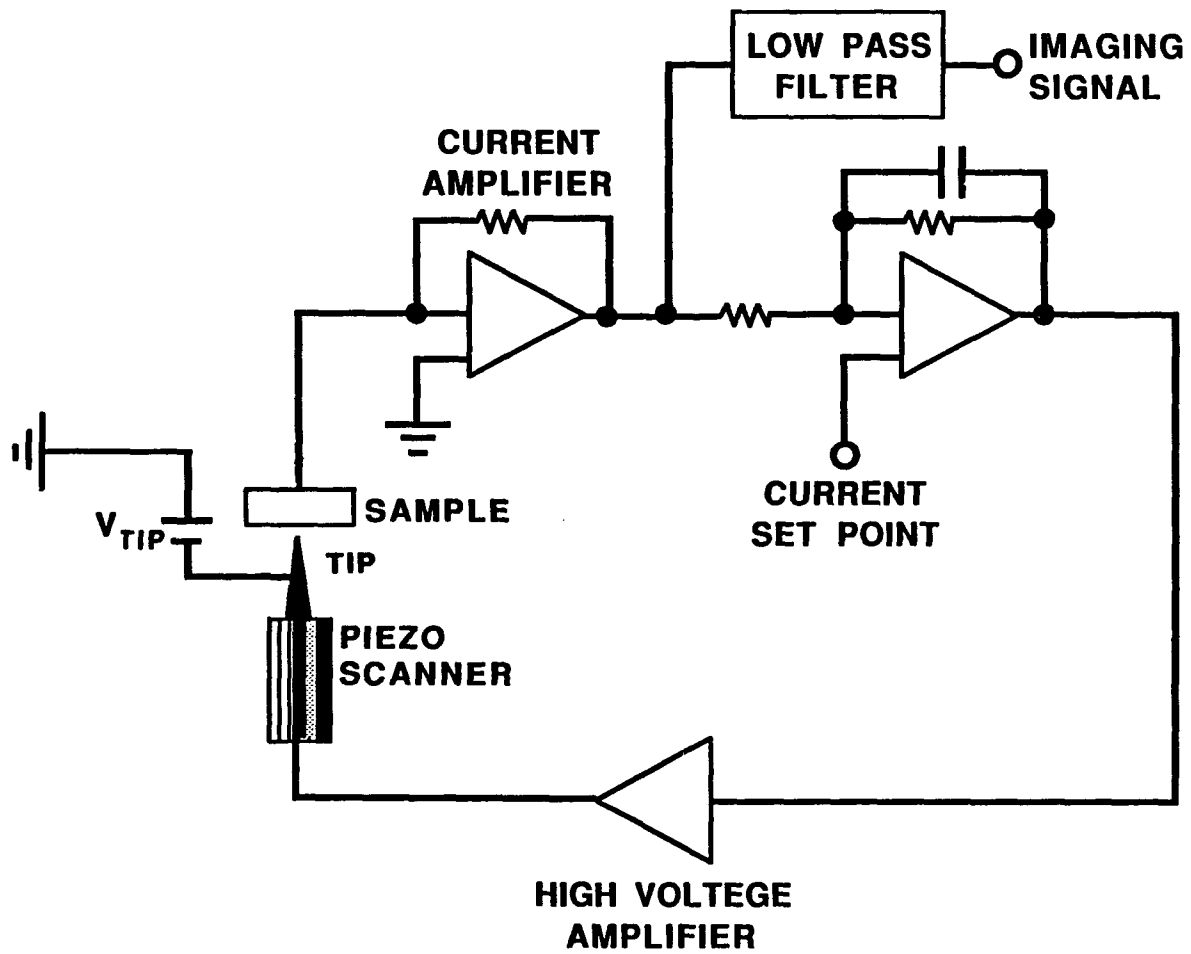


Figure 1.3 Schematic drawing of Feedback System for the Constant Height Mode.

Table 1.1. Advantages and disadvantages of STM modes of operation.

	<u>Constant Current</u>	<u>Constant Height</u>
<u>Advantages</u>	<ol style="list-style-type: none"> <li>1. Heights of surface features easily measured</li> <li>2. Can measure features of rough surfaces</li> </ol>	<ol style="list-style-type: none"> <li>1. Fast</li> <li>2. Not extremely vibration sensitive</li> </ol>
<u>Disadvantages</u>	<ol style="list-style-type: none"> <li>1. Slow</li> <li>2. Extremely vibration sensitive</li> </ol>	<ol style="list-style-type: none"> <li>1. Can only measure features of flat surfaces</li> </ol>

the surface. The most common of these methods are the line scan and the grey scale image.

### Discovery

The pioneering work of G. Binnig, H. Rohrer, Ch. Gerber, E. Weibel, and their collaborators at IBM Zurich Laboratories sparked the rapid growth of research in STM. In the first paper by Binnig et al. (1982), he describes obtaining images with atomic resolution, which was not obtainable by any other known method. He was able to obtain this type of resolution by using a rigid STM and isolating it from vibrations. However, the images were not always reproducible, and many people doubted their validity. It was not until they imaged the 7 x 7 reconstruction of a silicon surface (Binnig et al. 1983) that many people began to believe that they were indeed able to image surfaces on the atomic scale. It was quite amazing that they were able to obtain atomic resolution at all, considering that their procedure for making tips was only mechanical grinding.

The development of tunneling microscopy, however, was anticipated by Young et al. (1972) when they invented a device known as the topografiner, 10 years before the development of the STM. The topografiner uses the same underlying principles as the STM. They were able to achieve a resolution of 4000 Å in the lateral direction and 30 Å in the vertical direction with a field emission voltage of 50 V and 200 Å gap spacing. However, problems with blunt tips and the lack of vibration isolation prevented them from obtaining higher resolution.

### Theory

STM images appear to be simply direct topographs of the surface. Although this is not strictly correct, this view is adequate for most cases (Binnig et al. 1982). However, when atomic resolution imaging was discovered (Binnig et al. 1983) it became apparent that a more complex understanding of STM is required in the interpretation of the images.

In the early work with STM, the tunneling current and the images were analyzed on the basis of an analogy with the one-dimensional tunneling problem. The tunneling current under low voltage and temperature behaves as

$$I \propto \exp(-2\kappa s) \tag{1.1}$$

where  $I$  is the tunneling current,  $s$  is the tip-to-surface separation, and  $\kappa$  is the decay constant for the wavefunctions in the barrier. In the case of vacuum tunneling,  $\kappa$  is related to the effective local work-function  $\phi$  by

$$\kappa = \left[ \frac{\hbar}{2\pi} \right] (2m\phi)^{1/2}, \tag{1.2}$$

where  $m$  is the electron mass, and  $\hbar$  is Planck's constant.

For a typical decay constant of  $1 \text{ \AA}^{-1}$ , the current decreases by an order of magnitude when  $s$  is increased by  $1 \text{ \AA}$ . Therefore, height changes of  $0.1 \text{ \AA}$  can be easily detected. This is why images are interpreted as simply a contour of constant height above the surface.

However, there are some problems with this theory. The first problem is that it is not clear what exactly is the distance  $s$ . The second problem is associated with the fact that tunneling takes place between the two Fermi levels, that of the tip and that of the surface, which themselves may have a complex spatial structure. Therefore, the electronic structure of the tip and the surface may enter in a complex way. For these reasons, one needs to consider a full three-dimensional tunneling problem in the interpretation of STM images.

The tunneling current can be given to first order in terms of Bardeen's formalism by (Bardeen 1961)

$$I = \frac{(2\pi e)^2}{h} \sum_{\mu, \nu} (|M_{\mu\nu}|^2 f(E_\mu) [1 - f(E_\nu + eV)] \delta(E_\mu - E_\nu)) \quad (1.3)$$

where  $M_{\mu\nu}$  is the tunneling matrix element between the states  $\psi_\mu$  of the tip and  $\psi_\nu$  of the surface,  $f(E)$  is the Fermi function,  $V$  is the voltage applied across the barrier, and  $E_\mu$  is the energy of the state  $\psi_\mu$  in the absence of tunneling. Bardeen (1961) also showed that the tunneling matrix can be written as

$$M_{\mu\nu} = \frac{\hbar^2}{8\pi^2 m} \int dS (\psi_\mu^* \nabla \psi_\nu - \psi_\nu \nabla \psi_\mu^*) \quad (1.4)$$

where the integral is over any surface lying entirely within the vacuum (barrier) region separating the tip and the surface. The quantity in parentheses is the current operator. In theory, equations (1.3) and (1.4) are all that are necessary to calculate the tunneling current, and hence the STM image. However, in practice, several approximations are needed to derive an expression which permits practical

computation of the tunneling current.

Tersoff and Hamann (1985) showed that in the limit of small voltage and temperature the tunneling current can be written as

$$I = \frac{(2\pi e)^2 V}{h} \sum_{\mu, \nu} (|M_{\mu\nu}|^2 \delta(E_\nu - E_F) \delta(E_\mu - E_F)) \quad (1.5)$$

where  $E_F$  is the Fermi energy. However, the tunneling current makes no distinction between tip and surface, and ideally, one would like to relate the STM image directly to a property of the surface. Tersoff and Hamann (1985) observed that the tip properties could be taken out of equation (1.5) if the tip is replaced with a point probe and if the potential and wavefunction of the tip are arbitrarily localized. Then the tunneling current reduces to

$$I \propto e^2 V \sum_{\nu} |\psi_{\nu}(\mathbf{r}_0)|^2 \delta(E_\nu - E_F) = e^2 V \rho(\mathbf{r}_0, E_F) \quad (1.6)$$

where  $\mathbf{r}_0$  is the center of curvature of the tip wavefunction  $\psi_{\mu}$  and  $\rho(\mathbf{r}_0, E_F)$  is the local density of states (LDOS) at the position of the point probe and energy  $E_F$ . Under these conditions the tunneling conductance is

$$\sigma \propto \rho(\mathbf{r}_0, E_F) \quad (1.7)$$

which is independent of voltage in the limit of small voltage.

Making these assumptions, the STM image has a straightforward interpretation. The current is proportional to the surface LDOS at  $E_F$  at the tip position, and consequently, the tip path maps out contours of constant Fermi-level LDOS of the surface. Tersoff and Hamann (1985) also showed that this result could be extended to a tip having an arbitrary size, as long as the tip wavefunction at  $E_F$  could be represented by an s-wave wavefunction, and  $r_0$  is taken as the center of curvature of the tip wavefunction.

Although many of these approximations seem rather severe, the accuracy of equation (1.7) for an atomically sharp tip has been directly confirmed by Lang (1986a), who performed essentially exact calculations using real wavefunctions of a tip and a surface.

### STM Applications

STM is no longer a new field. Many surfaces have been studied under many different conditions. The first application of the STM was used to study the reconstruction of metal and semiconductor surfaces in an ultrahigh vacuum environment. G. Binnig et al. (1984) showed that the  $1 \times 5$  reconstruction of Au(100) is not the same all over the plateaus, but rather there are subtle variations in the atom positions at different locations. The ability of the tunneling microscope to see these subtle variations within surface reconstruction makes the STM a very powerful tool. More recently the applications of STM have been expanded to include the study of surface chemistry (Hosler et al. 1986), biology (Baro' et al. 1985), and electrochemistry (Coleman et al. 1985). Experiments have been performed in air (For example Sarid et al. 1988a), aqueous solution (Sonnenfeld and

Hansma 1986), and liquid nitrogen (Sonnenfeld and Shardt 1986). The STM has also been used to study superconductivity (Elrod et al. 1984) and charge density waves (Sonnenfeld and Shardt 1986).

D. W. Abraham et. al (1986a) showed that lithography can be done by simply scratching the surface with the tip of the STM. The same group also found that it was possible to deposit materials from the tip onto the surface, and thus it was possible to use the tip to both deposit and remove materials. Surface diffusion could be observed with the STM on a time scale of minutes after the material was transferred. Another recent development is the use of a STM to plot potential distributions across a surface with microscopic resolution. The STM developed by Muralt and Pohl (1986) can measure the surface topography and potential distribution at the same time.

The idea of STM has been extended in the development of the atomic force microscope which can detect the van der Waals forces between atoms and the magnetic force microscope which images magnetic domains on the nanometer scale. P. K. Hansma and J. Tersoff (1987) have published an excellent review that gives a general account for the many experimental and theoretical results that have occurred in STM in the past few years.

### Organization of the Thesis

In chapter 2, our STM system is described, and a graphite image obtained with our system is presented. Images of layered-structure semiconductors are presented in Chapter 3. Spectroscopic measurements on the layered-structure semiconductors which measure the bandgap and give a representation of the density of

states (DOS) are also presented. Images of layered-structure semiconductor clusters are presented in Chapter 4. The results obtained with the clusters are compared to those of the bulk material in order to obtain an understanding of the size-dependent properties of the material. Future STM research is discussed in Chapter 5.

## CHAPTER 2

### OUR STM SYSTEM

Our STM operates in air at room temperature in the constant height mode (Sarid et al. 1988a). Figure 2.1 is a schematic drawing of the STM system used in this study. The piezo electric tube provides displacement of the tip at a rate of  $75 \text{ \AA}$  per volt (calibrated relative to graphite) in the x and y directions (in the plane of the surface), and displacement of  $50 \text{ \AA}$  per volt in the z direction (perpendicular to the surface). The tip is raster scanned in the x direction with a 1 KHz sine wave, and is then slowly scanned in the y direction with a 4 Hz ramp. The high speed x scan must have a sinusoidal waveform rather than a triangular waveform in order to avoid high-frequency components which could excite mechanical resonances (8 kHz in the x and y directions and 40 kHz in the z direction) in the piezoelectric tube which holds the tip. To avoid any effects from possible hysteresis in the piezoelectric tube, a blanking circuit is used to acquire data only in one scan direction; e.g., only left to right and top to bottom. The tip is kept at a constant average height through the use of a feedback network, and changes in the tunneling current are monitored. To demonstrate the quality of our STM system, a typical graphite image (See Fig. 2.2) is presented. The lattice parameters and the electronic structure of graphite are well known. Therefore, graphite is an ideal candidate for testing the quality of the STM system, as well as calibrating the piezoelectric tube scanner.

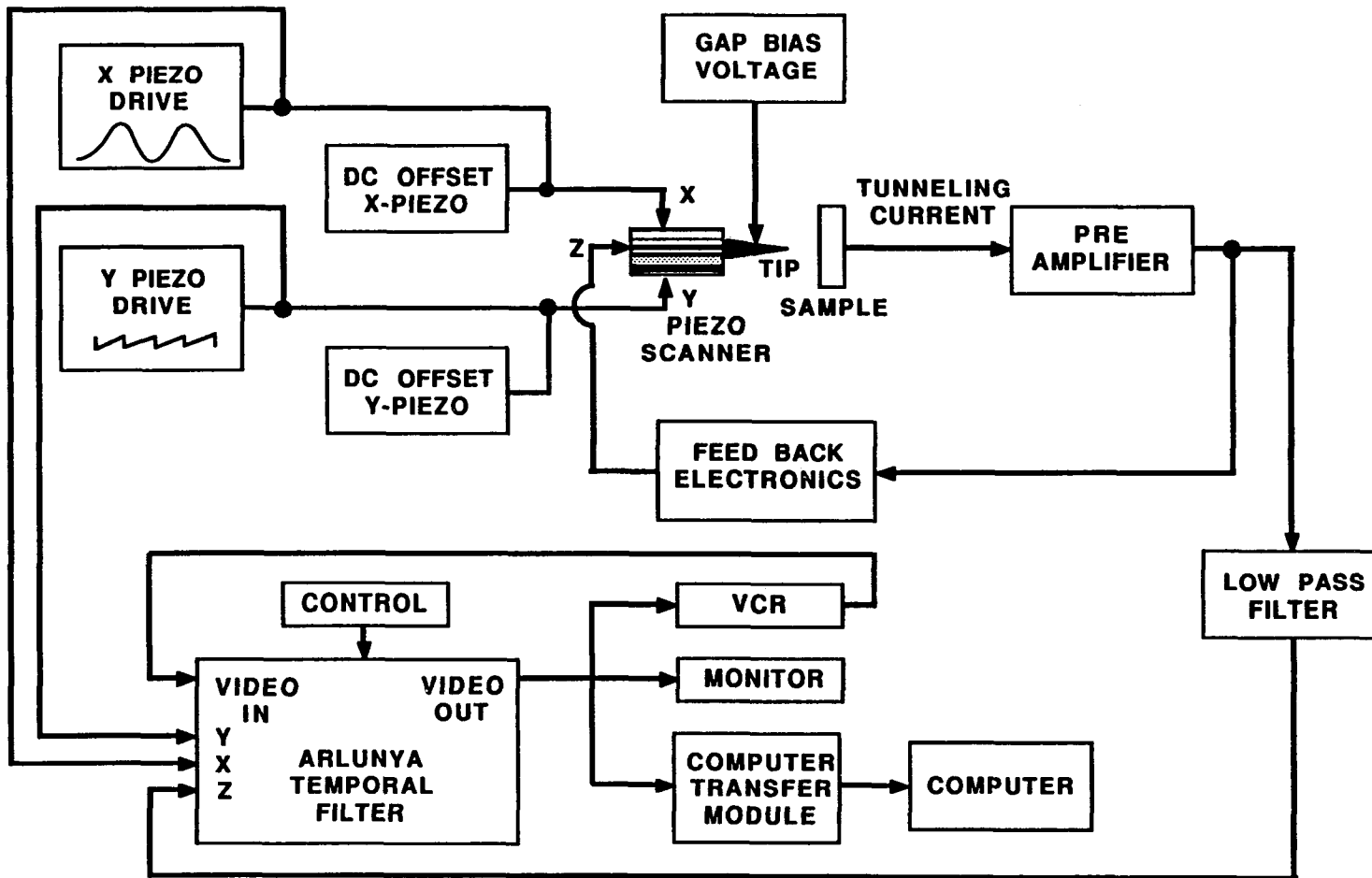
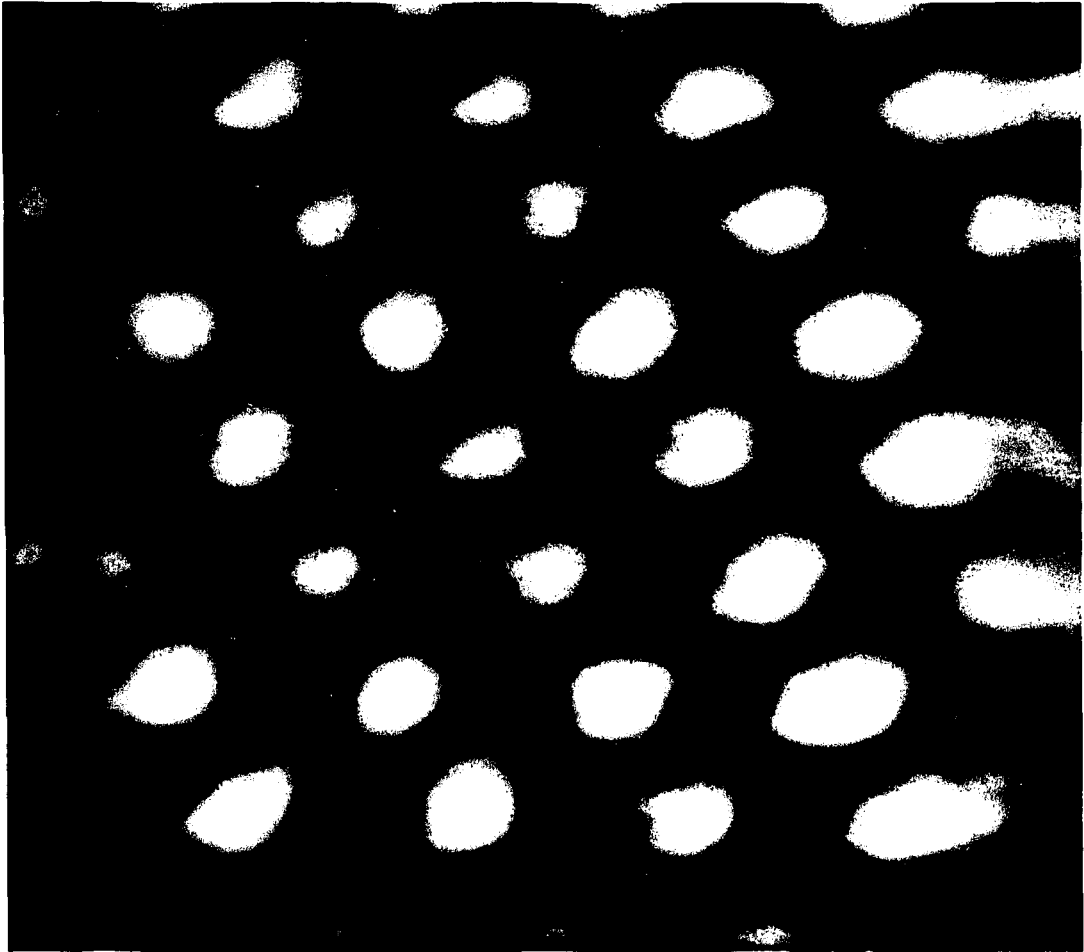


Figure 2.1 Schematic drawing of the STM system used in this study.

Figure 2.2 Grey scale image of the surface of graphite. The image was obtained with a sample bias of 50 mV and represents an area of 15 Å X 15 Å.



### Image Processing

While scanning the surface, the x, and y scan signals and the z signal (tunneling current) are sent to an Arlunya TF5111 image processor<sup>1</sup> (Princeton Electronics Products, North Brunswick, NJ) which converts the scan rates to video rates so that the images can be viewed in real time on a monitor. At the same time, the image is sent to a video cassette recorder (VCR) so that one can make "movies" of atomic images. The Arlunya also temporally filters the images making them easier to view and interpret, and provides means to send the images to a computer where further processing can take place. To improve the quality of our images, we display them on a monitor whose screen is covered by a thin sheet of tracing paper which acts as a low pass filter. This serves to defocus the the image, and thereby spatially filter it. The image is recorded with a video camera and is transferred to a second VCR. Figure 2.3 demonstrates how the spatial filtering improves the image quality. All of the images presented in this thesis have been filtered in this manner.

---

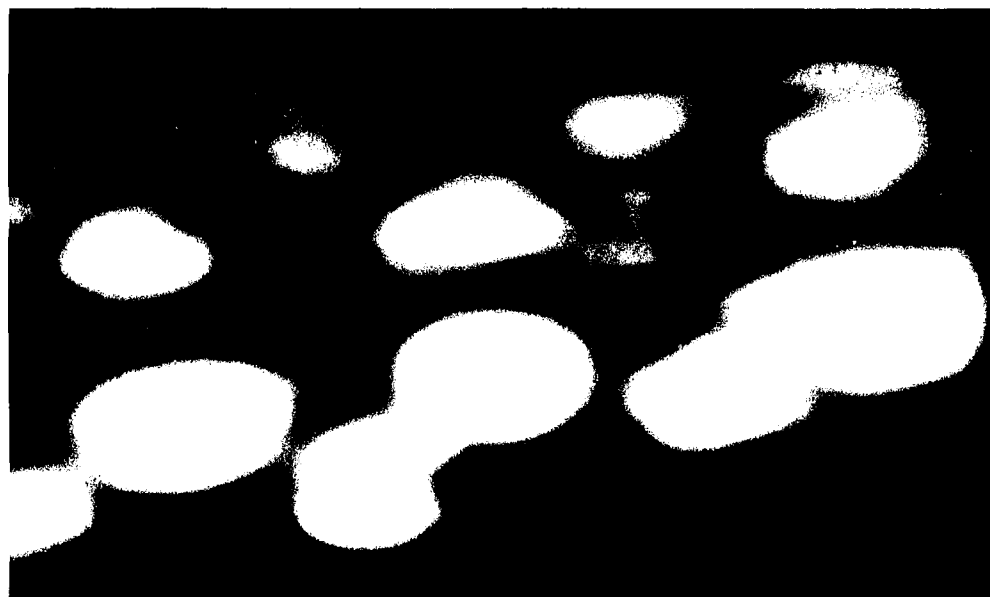
1. Commercial materials and equipment are identified in order to adequately describe the procedure. This identification does not imply endorsement by the University of Arizona nor does it imply that the identified material or equipment is the best available for the purpose.

Figure 2.3 Grey scale image of a cluster on the surface of graphite. Each image was obtained with a sample bias of 50 mV and represents an area of 15 Å X 9 Å. (a) and (b) show the cluster before and after spatial filtering, respectively.

(a)



(b)



### Vibration Isolation

There are two key factors to success in obtaining atomic resolution with a STM. They are excellent vibration isolation and atomically sharp tips. STM signals are very small and can easily be buried in noise caused by mechanical and acoustical vibrations, and it is therefore necessary to isolate the STM from these vibrations. The extent of vibration isolation necessary to obtain good atomic resolution images depends on the mode of operation of the STM. In the constant current mode, the x scan frequency, and therefore the STM signal, is on the order of typical building vibrations, i.e. 20 Hz, and the signal will be nearly impossible to extract from the noise caused by these vibrations. A passive vibration isolation system with excellent attenuation at typical building resonances is necessary to combat this problem. This can be accomplished by placing the STM on a large mass that is hung from the ceiling by rubber springs which stretch several inches.

In the constant height mode, the x scan frequency is well above the building resonances, so one mainly has to worry about high frequency vibrations. Our STM head, which was purchased from the Tunneling Microscope Company<sup>2</sup> (Menlo Park, CA), consists of stainless steel plates separated by viton tubing and provides excellent vibration isolation from high frequency noise. We found that hanging the STM from the ceiling with rubber straps provided as much vibration isolation

---

2. Commercial materials and equipment are identified in order to adequately describe the procedure. This identification does not imply endorsement by the University of Arizona nor does it imply that the identified material or equipment is the best available for the purpose.

as placing our STM on a floating granite table.

In recent years, it has become clear that increasing the rigidity of microscopes can be more conveniently achieved than perfecting a vibration isolation system. In manufacturing microscopes, the trend has been toward compactness and simplicity. It is very important to combine a rigid microscope with an excellent vibration isolation system in order to achieve high resolution images.

### Tip Preparation

To be able to resolve individual atoms, the effective tip radius needs to be on the order of the atomic spacing. Theoretically, the tips are required to consist of one single atom. Our method of tip preparation, which is commonly used, is to electrochemically etch a 1 cm long tungsten wire in a 5 molar solution of KOH with a 7 V dc voltage applied between the wire and the solution. Etched wires have a typical radius in the range of 0.1-10  $\mu\text{m}$  (Hansma and Tersoff 1987). However, Hansma and Tersoff (1987) state that these wires often produce atomic resolution images without any further processing, indicating that at least one atomically sharp tip is protruding from the relatively dull end.

After the wire is etched, there is still a small amount of current flowing between the wire and the solution which will dull the tip. It is therefore important to stop this current flow immediately after the tip is etched. To accomplish this, a circuit has been designed by Kevin Johnson, an electrical engineering student at the University of Arizona, that would sense the sudden drop in current that occurs when the wire is etched and would then stop any remaining current from flowing through the wire.

The wire is then removed from the etching system, and the tips are examined under a microscope that has a magnification of 200. If the ends of the tips appear sharp (no tip radius could be seen) then we place the tips into our STM system to see if they produce atomic resolution images. Tips which appear stubby to the naked eye tend to work better than tips which have long hair-like ends because they are less likely to be affected by the dragging force caused by air currents and the frictional force which exists between the tip and the surface.

## CHAPTER 3

## BULK LAYERED-STRUCTURE SEMICONDUCTORS

With a STM one can obtain information about the surface of a structure, which in many cases differs from that of the bulk. In this respect, semiconductors with layered-structures offer a unique opportunity for STM since there are no dangling bonds at the basal plane surfaces of these materials (Wieting and Schluter 1979, Reidel 1986), and consequently, the "atomic" images obtained by STM reflect the symmetry that also exists in the bulk (no reconstruction is required for minimizing the local energy).

Previous STM work on layered-structure semiconductors include imaging of  $\text{NbS}_2$ ,  $\text{NbSe}_2$ , and  $\text{GaSe}$ , and imaging and measurements of charge density waves in  $\text{TaS}_2$  and  $\text{TaSe}_2$  (Coleman et al 1985, Tokumoto and Bando 1987, Slough et al. 1986, Bando et al. 1986, Humbert et al. 1987). Recently, Stupian and Leung (1987) have presented images of  $\text{MoS}_2$  with atomic resolution obtained with a sample biased negatively with respect to the tip, while images of  $\text{MoS}_2$  with the sample biased positively with respect to the tip were obtained by Weimer et. al. (1988). Atomic resolution images of  $\text{MoS}_2$  were also obtained with an atomic force microscope by Albrecht and Quate (1988).

As part of a study on metal dichalcogenides, which consist of a layer of metal atoms sandwiched between chalcogenide atoms, two group IVB transition metal dichalcogenides,  $\text{MoS}_2$  and  $\text{WSe}_2$ , which are technologically important for energy conversion and catalysis (Tributsch 1982), as well as a group IVA non-transition metal dichalcogenide  $\text{SnS}_2$  (Sarid et al. 1988b) were investigated by STM. Furthermore,  $\text{MoS}_2$  and  $\text{WSe}_2$  are highly photosensitive in the entire visible and

near infrared spectral region, and unlike CdS and CdSe, for example, MoS<sub>2</sub> and WSe<sub>2</sub> exhibit good chemical stability with above bandgap illumination. MoS<sub>2</sub>, WSe<sub>2</sub>, and SnS<sub>2</sub> are all layered-structure semiconductors whose lattice parameters and energy gaps are listed in Table 3.1 (Wieting and Schluter 1979, Tributsch 1982, Evans 1976). They offer the opportunity to act as substrates which can be selectively decorated with a variety of adsorbates. The freshly exposed basal planes of these metal dichalcogenides are chemically inert, and their surface analysis demonstrates submonolayer concentrations of carbon and oxygen. This situation remains true even for crystals which have been immersed in solutions and subsequently withdrawn and analyzed (Stickney et al. 1984).

### Images

Images of the layered-structure semiconductors were obtained with our STM operated in the constant height mode. A sample-to-tip bias of -1 V or +1 V, typically, was applied, and an average tunneling current of 5 nA was measured (Sarid et al. 1988b). The images were then stored on a VCR and sent to a computer for further analysis.

The three crystals used in the experiments were: (a) a naturally grown crystal of MoS<sub>2</sub>, excavated in Arizona, (b) a WSe<sub>2</sub> Nb doped crystal and (c) a SnS<sub>2</sub> crystal. All of the crystals yielded high quality images with atomic resolution for both bias voltage polarities. Figures 3.1, 3.2, and 3.3 show typical atomically resolved grey scale images of MoS<sub>2</sub>, WSe<sub>2</sub>, and SnS<sub>2</sub>, respectively, for a positive sample bias. Figures 3.4, 3.5, and 3.6 show typical atomically resolved grey scale images of MoS<sub>2</sub>, WSe<sub>2</sub>, and SnS<sub>2</sub>, respectively, for a negative sample bias. The

Table 3.1. Lattice parameters and energy gaps of bulk layered-structure semiconductors.

<u>Material</u>	<u>a</u>	<u>c</u>	Optically Measured
			<u>Energy gap</u>
MoS <sub>2</sub>	3.16 Å	12.3 Å	1.13 - 1.6 eV
WSe <sub>2</sub>	3.28 Å	12.95 Å	1.16 - 1.4 eV
SnS <sub>2</sub>	3.64 Å	5.86 Å	2.2 eV

Figure 3.1 Atomically resolved image of MoS<sub>2</sub> obtained with a sample bias of 1 V. The image represents an area of 22 Å X 22 Å.

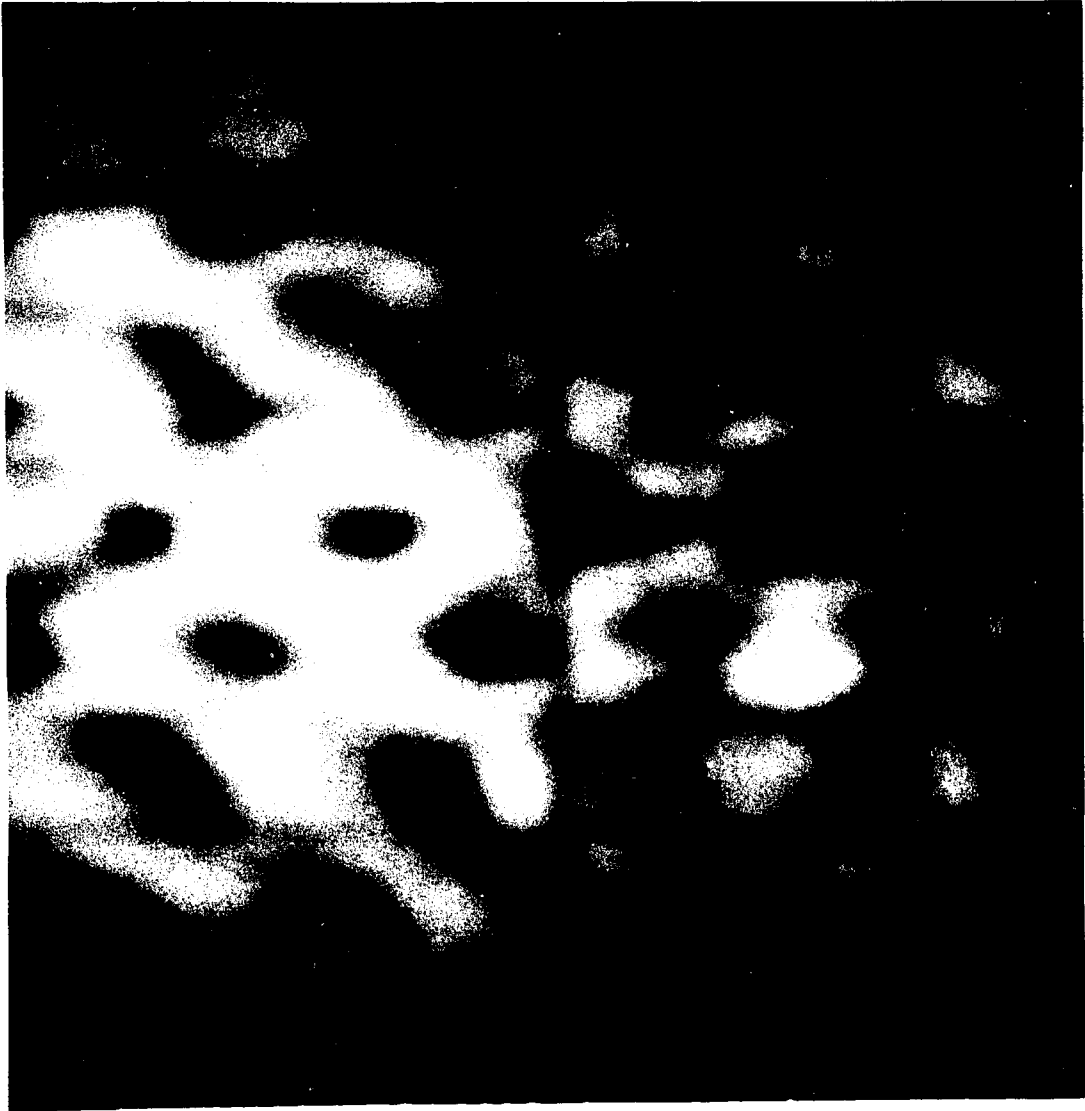


Figure 3.2 Atomically resolved image of  $\text{WSe}_2$  obtained with a sample bias of 0.6 V. The image represents an area of  $18 \text{ \AA} \times 18 \text{ \AA}$ .

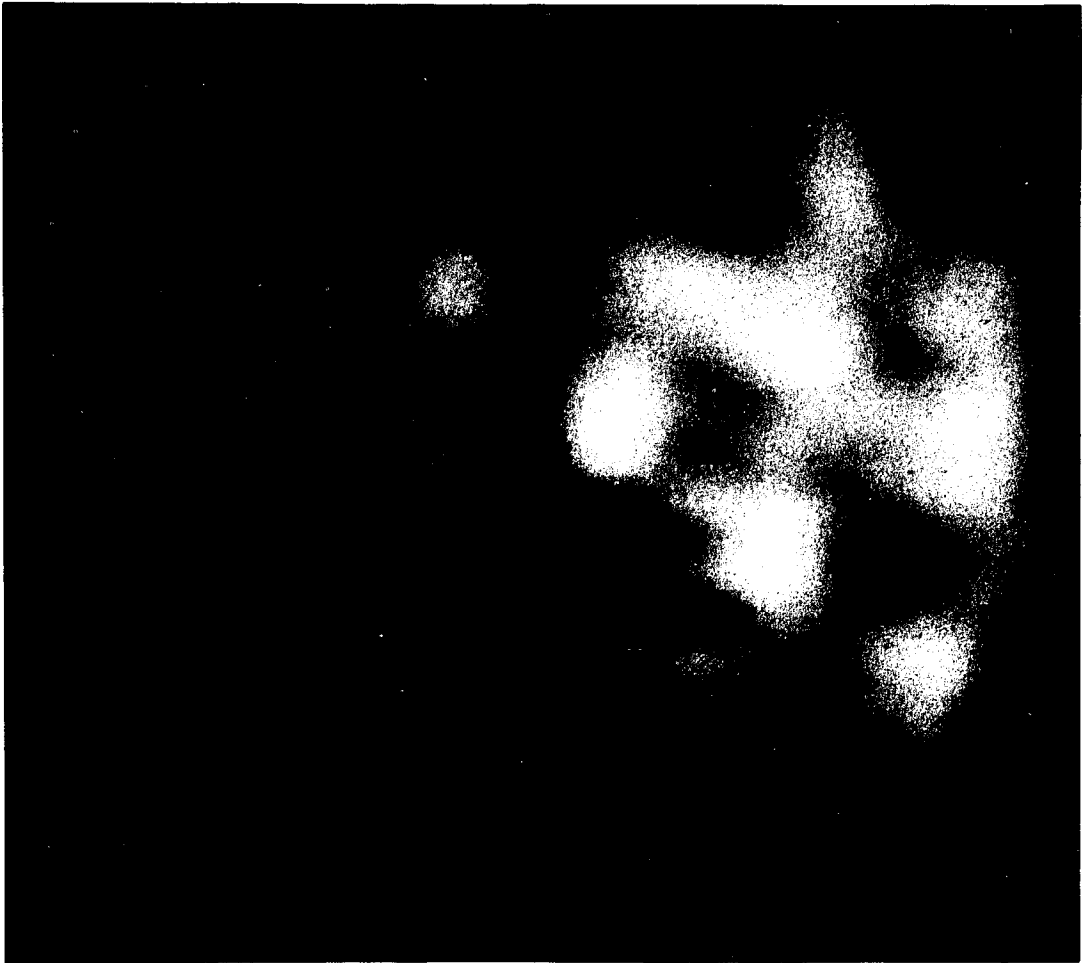


Figure 3.3 Atomically resolved image of SnS<sub>2</sub> obtained with a sample bias of 0.6 V. The image represents an area of 18 Å X 18 Å.



Figure 3.4 Atomically resolved image of MoS<sub>2</sub> obtained with a sample bias of -1 V. The image represents an area of 22 Å X 22 Å.

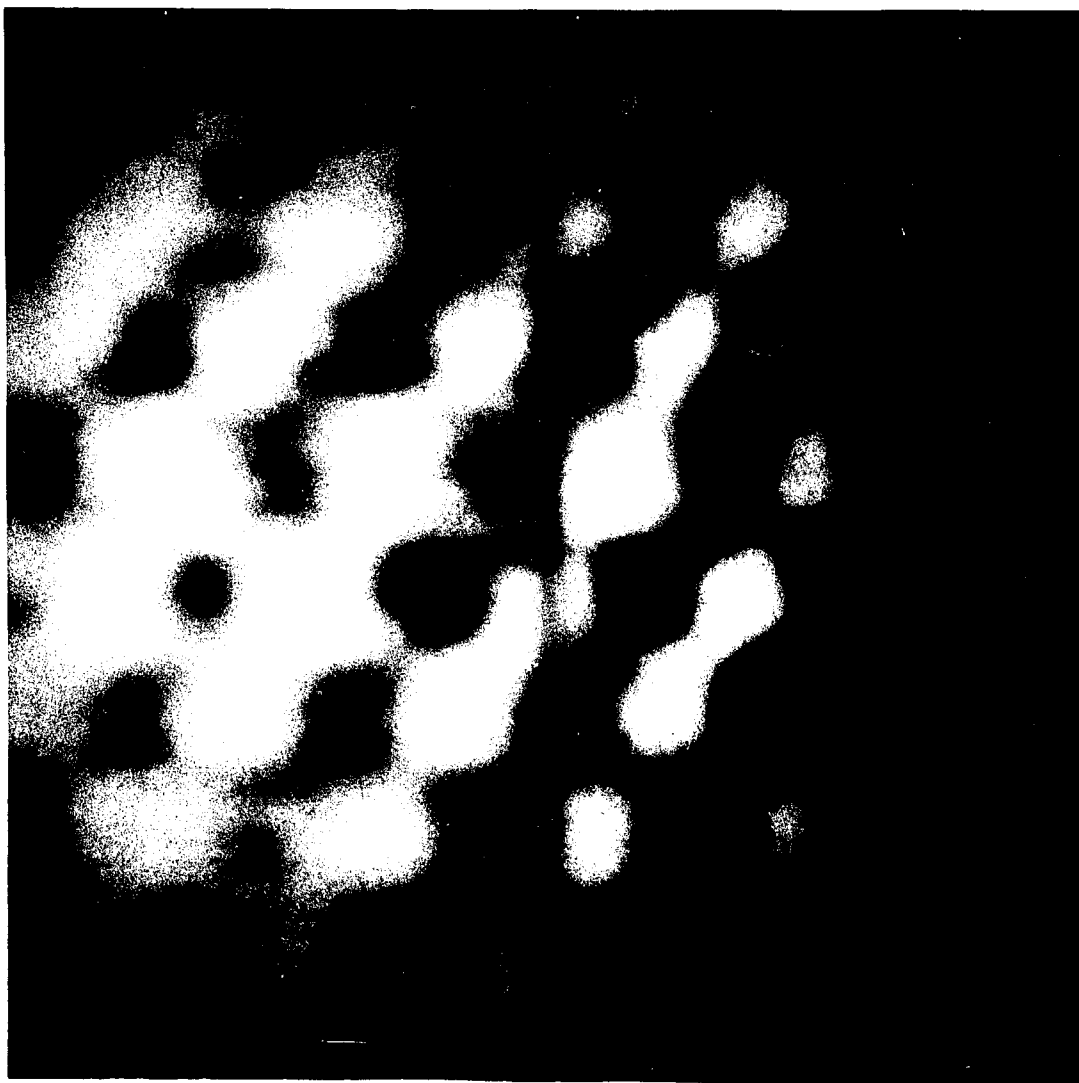


Figure 3.5 Atomically resolved image of  $\text{WSe}_2$  obtained with a sample bias of  $-0.6 \text{ V}$ . The image represents an area of  $18 \text{ \AA} \times 18 \text{ \AA}$ .

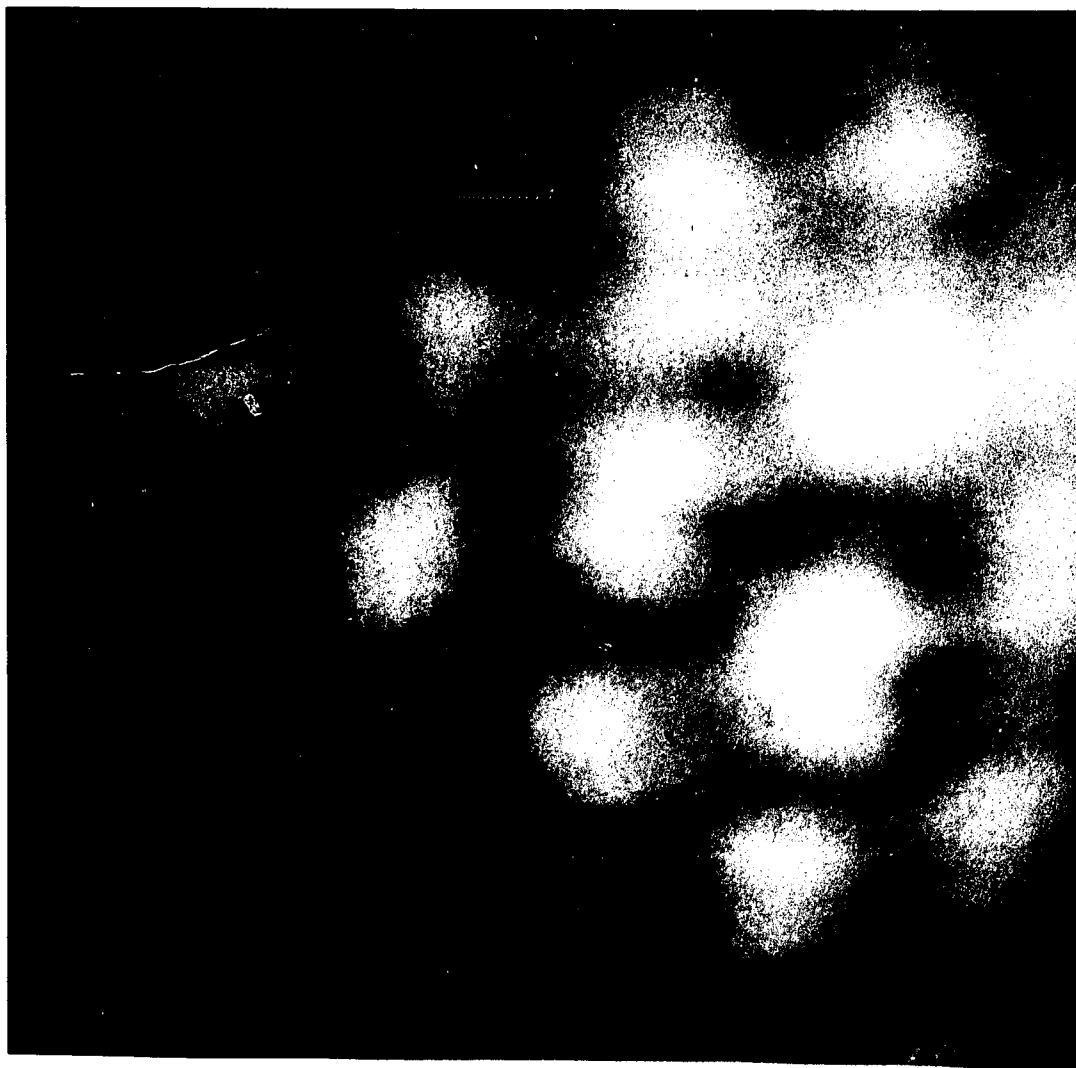


Figure 3.6 Atomically resolved image of SnS<sub>2</sub> obtained with a sample bias of -0.6 V. The image represents an area of 18 Å X 18 Å.



hexagonal symmetry of these structures is clearly observed in these images, and the average lattice spacing was measured to be 3.26 Å, 3.48 Å, and 3.74 Å for MoS<sub>2</sub>, WSe<sub>2</sub>, and SnS<sub>2</sub>, respectively, which is within 6 percent of the known values. The limited accuracy in the lattice spacing is probably due to the finite signal-to-noise ratio of our experimental system.

### Density of States Measurement

Spectroscopic measurements by STM consist essentially of bringing a tip 5 to 10 Å away from a surface, applying a voltage (V) between the tip and the surface, and measuring the resulting tunneling current (I). The differential conductance  $dI/dV$  yields a measure of the surface density of states ( Tersoff and Hamann 1983, Baratoff 1984, Selloni et al. 1985, Lang 1986b). However Feenstra et al. (1987) showed that the differential conductance is exponentially dependent both on the bias voltage and the tip-to-surface separation, and these effects tend to mask the relevant density of states features. To eliminate these dependencies, Feenstra et al. (1987) suggested that one compute the ratio of differential to total conductance  $(dI/dV)/(I/V) = d(\ln I)/d(\ln V)$  which was shown experimentally to cancel out the exponential dependence on voltage and separation in the spectroscopic measurements. The tunneling current is given by ( Tersoff and Hamann 1983, Baratoff 1984, Selloni et al. 1985, Lang 1986b)

$$I \propto \int_0^{eV} \rho(E) T(E, eV) dE, \quad (3.1)$$

where  $\rho(E)$  is the surface density of states of the sample, and  $T(E, eV) = \exp(-2\kappa s)$  is the transmission probability of the electron tunneling through the air gap. Here  $s$  is the tip-to-surface separation and  $\kappa = \kappa(E, eV)$  is the inverse decay length given by (Feenstra et al. 1987)

$$\kappa = \left[ \left[ \frac{8\pi^2 m}{h^2} \right] (U - E_{\text{total}}) + k_{\text{trans}}^2 \right]^{1/2} \quad (3.2)$$

where  $U = (\phi_1 + \phi_2 + eV)/2$  is the average barrier height between tip and sample having work-functions  $\phi_t$  and  $\phi_s$  respectively, and  $V$  is the voltage applied to the sample. Taking the derivative of  $I$  with respect to  $V$ , one finds (Feenstra et al. 1987)

$$\frac{dI}{dV} \propto e\rho(eV)T(eV, eV) + e \int_0^{eV} \rho(E) \left[ \frac{d}{d(eV)} \right] [T(E, eV)] dE. \quad (3.3)$$

Consequently (Feenstra et al. 1987),

$$\frac{d(\ln I)}{d(\ln V)} = \frac{\rho(eV) + \int_0^{eV} \left[ \frac{\rho(E)}{T(eV, eV)} \right] \left[ \frac{d}{d(eV)} \right] [T(E, eV)] dE}{\left[ \frac{1}{eV} \right] \int_0^{eV} \rho(E) \left[ \frac{T(E, eV)}{T(eV, eV)} \right] dE}. \quad (3.4)$$

Since  $T(E, eV)$  and  $T(eV, eV)$  appear as ratios in this equation, their exponential dependencies on  $s$  and  $V$  tend to cancel.

From Eq. 3.4, one observes that a measure of  $d(\ln I)/d(\ln V)$  yields the normalized density of states at the surface of the sample plus a background term. Therefore, curves of  $d(\ln I)/d(\ln V)$  plotted as a function of bias voltage, measured at the surface, approximately map the local density of states both at the surface (Feenstra et al. 1987) and inside the bulk (no surface states exist along cleavage planes in layered semiconductors). It should also be noted, that STM is capable of mapping the valence band and conduction band density of states separately, in contrast to optical absorption spectra which yield only the joint density of states (Sarid et al. 1988b). Another important difference between STM and optical measurements is that in the latter the light excites electron-hole pairs, and the absorption spectrum, therefore, contains the Sommerfeld factors as well as excitonic features. One can further view the difference between optical excitation and a tunneling process by considering a potential well having discrete energy levels. In optical processes, the electron has to climb a ladder of energy levels "vertically", while in tunneling processes it escapes the potential well "sideways" by leakage (Sarid et al. 1988b). Thus, when the sample-to-tip bias is negative, and electron from the highest valence band of the sample tunnels directly into the tip. For a positive sample-to-tip bias, an electron from the tip tunnels directly into the bottom conduction band of the sample, after which it thermalizes into the top valence band.

For the measurement of  $I$  vs.  $V$  (Feenstra et al. 1987, Baratoff et al. 1986, Tersoff and Hamann 1983, Tromp et al. 1986, Hansma and Tersoff 1987), a triangular sample-to-tip bias voltage with an amplitude of about 1 V and a frequency of 100 Hz was applied. The measurements are carried out without raster scanning, and the tip is allowed to drift slowly across the sample surface. The feed-

back network that drives the z-axis of the piezoelectric tube is fed by a lock-in amplifier which filters the tunneling current. Curves of the unfiltered tunneling current as a function of the triangular bias voltage are recorded by a Gould model 4070 digital storage oscilloscope, and subsequently transferred to a computer for further analysis.

As shown by Feenstra et al. (1987), curves of  $d(\ln I)/d(\ln V)$  plotted as a function of  $V$  provide a measure of the local density of states. Figures 3.7, 3.8, and 3.9 are plots of  $I$  and  $d(\ln I)/d(\ln V)$  versus  $V$  for  $\text{MoS}_2$ ,  $\text{WSe}_2$ , and  $\text{SnS}_2$ , respectively. One observes an energy gap of 1.35 eV for  $\text{MoS}_2$ , 1.2 eV for  $\text{WSe}_2$ , and 0.75 eV for  $\text{SnS}_2$ . It is difficult however, to see any structure in the density of states due to our limited range in bias voltage. The agreement between STM and optical measurements for  $\text{MoS}_2$  and  $\text{WSe}_2$  is good (See Table 3.1), while the discrepancy in the two measurements for  $\text{SnS}_2$  may be attributed to the high doping levels of our samples.

Feenstra et al. (1987) observed that when the sample is biased positively  $T(E, eV) < T(eV, eV)$ , the background term in equation 3.4 is small compared to the normalized density of states term, and one obtains a measure of the density of states. When the sample is biased negatively,  $T(E, eV) > T(eV, eV)$ , the background term can be quite large compared to the normalized density of states term, so that the observed density of states is reduced by that amount. Consequently, it should be easier to tunnel into a semiconductor than to tunnel out. Our experimental results, however, show that with some materials it is easier to tunnel out of the sample than to tunnel in.

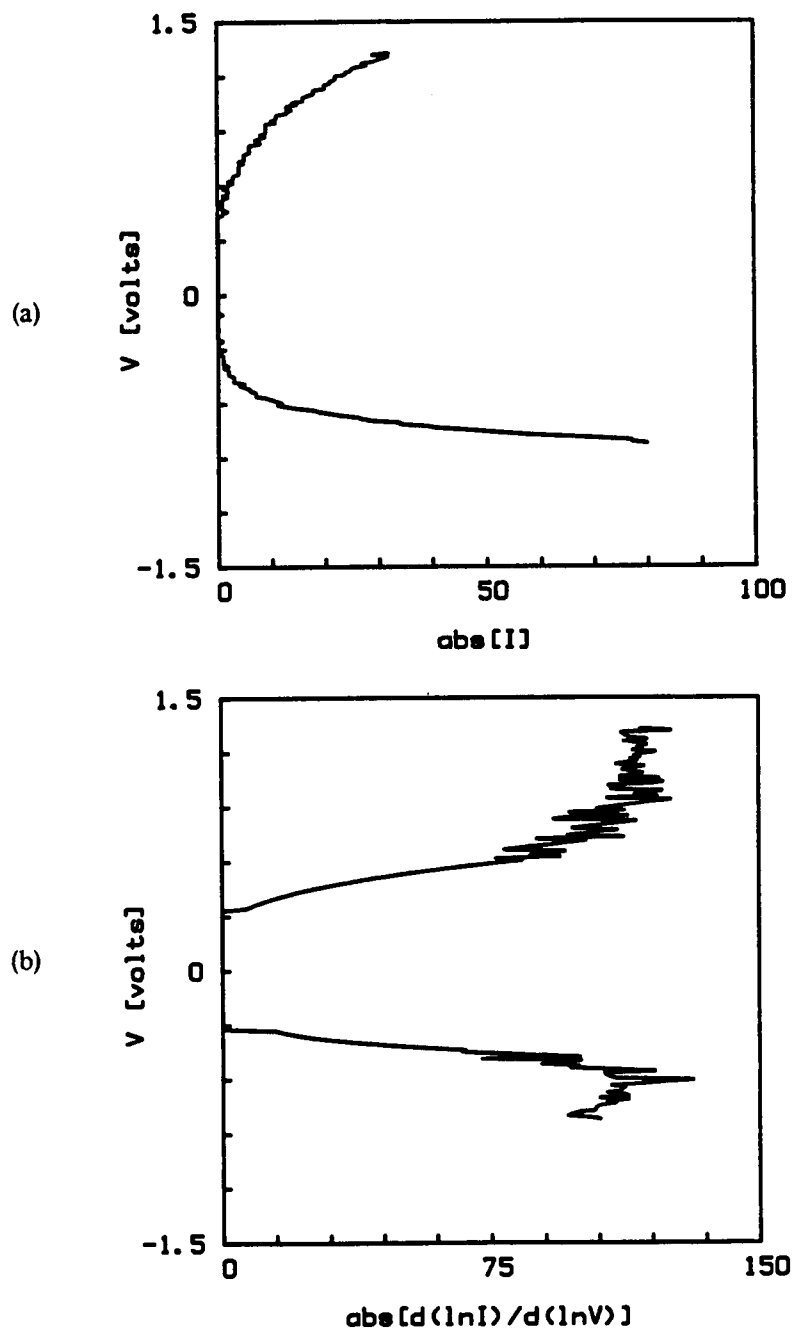


Figure 3.7 Plots of (a)  $I$  and (b)  $d(\ln I)/d(\ln V)$  in arbitrary units as a function of sample bias voltages in the range of  $-0.825 \text{ V} < V_{\text{bias}} < 1.3 \text{ V}$  for  $\text{MoS}_2$ . Note the existence of an energy gap of  $0.75 \text{ eV}$ .

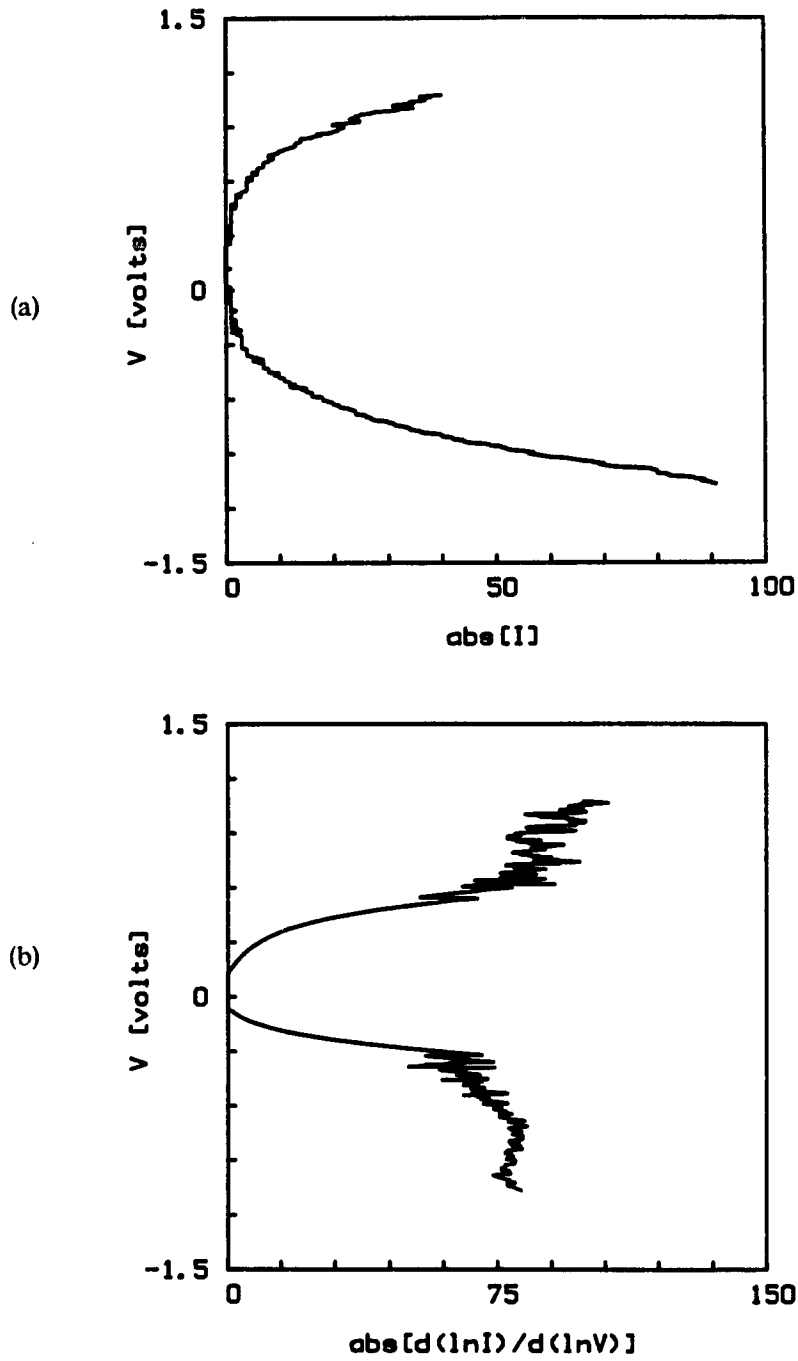


Figure 3.8 Plots of (a)  $I$  and (b)  $d(\ln I)/d(\ln V)$  in arbitrary units as a function of sample bias voltages in the range of  $-1.075 \text{ V} < V_{\text{bias}} < 1.075 \text{ V}$  for  $\text{WSe}_2$ . Note the existence of an energy gap of  $0.43 \text{ eV}$ .

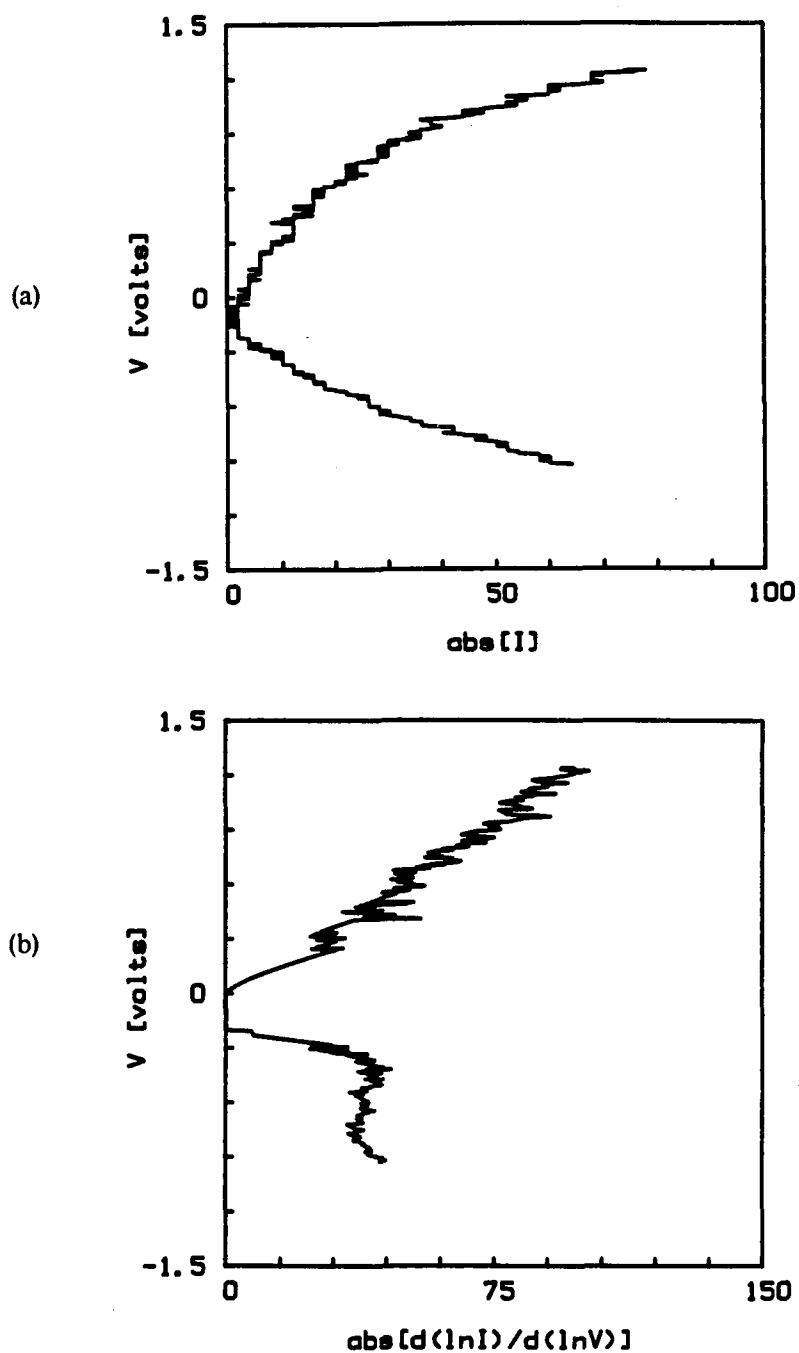


Figure 3.9 Plots of (a)  $I$  and (b)  $d(I)/d(V)$  in arbitrary units as a function of sample bias voltages in the range of  $-0.935 \text{ V} < V_{\text{bias}} < 1.24 \text{ V}$  for  $\text{SnS}_2$ . Note the existence of an energy gap of  $0.15 \text{ eV}$ .

## Results and Conclusions

We were able to obtain atomically resolved images of  $\text{MoS}_2$ ,  $\text{WSe}_2$ , and  $\text{SnS}_2$  for both bias polarities. Our measurements of lattice constants were close to the expected values, indicating that STM is an accurate means for measuring lattice spacings of surfaces of layered-structure semiconductors. Curves of  $I$  and  $d(\ln I)/d(\ln V)$  versus  $V$  were plotted and the existence of energy gaps was observed for all the layered-structure semiconductors. The energy gaps measured with the STM agreed with gaps measured by optical methods for  $\text{MoS}_2$  and  $\text{WSe}_2$ , while there was some discrepancy between the two measurements for  $\text{SnS}_2$ . To observe all the features which might be present in the conduction and valence bands of these materials, one would need to have a larger range of bias voltages. This requires a system whose feedback network can remain stable when larger tunneling currents are produced as a result of the larger bias range. Currently, our feedback network is unable to produce the required stability. Preferably, the density of states of a material should be measured in ultra-high vacuum in the constant current mode to assure stability and accuracy of the system. For some materials it may even be necessary to cool the samples to reduce the thermal vibrations, and therefore, sharpen the energy peaks in the density of states measurements. Once the density of states of a sample is measured, one can measure the bandgap of the material and can identify those energies which are involved in the tunneling and subsequently identify the material itself. It was also observed that certain materials produce larger tunneling currents for a given bias polarity, indicating that they have a preferred tunneling direction.

## CHAPTER 4

### SEMICONDUCTOR CLUSTERS

Semiconductor clusters imbedded in dielectric solids or liquids exhibit third order nonlinear susceptibilities which can be used for optical signal processing applications (Peyghambarian et al. 1986, Sarid et al. 1986). When the dimension of a cluster becomes smaller than the de Broglie wavelength of the electron in the cluster, the quantum confinement of the charge carriers blue shifts the bandgap (Rossetti et al. 1984a and 1984b, Weller et al. 1985), modifying both the linear and nonlinear optical responses.

The structural, optical and electronic properties of these clusters are topics of intense activity today. Composed of a few to several hundreds of atoms, clusters often exhibit features not seen in their bulk analogs (Sarid et al. 1988a). In small silicon clusters, for example, band structure calculations indicate that silicon atoms bind with a coordination much higher than the four-fold tetrahedral arrangement found in the bulk. One of the most important issues in cluster science has to do with the way bulk properties of materials (ie., lattice parameters, metallic work functions, semiconductor bandgaps) evolve from those of the atom as a function of cluster size. To achieve an understanding of these size-dependent materials properties one would like to experimentally determine the structure of clusters containing differing numbers of atoms (Bryant et al. 1986, Abraham et al. 1986b). While many workers have succeeded in generating well-resolved cluster size distributions using molecular beam techniques, the small concentration of species has precluded any direct experimental determination of their structure using optical techniques.

### Image of an Isolated Cluster on Graphite

As a first try, the structure of  $\text{BiI}_3$  clusters in colloidal suspensions on which we had previously demonstrated four-wave mixing and phase conjugation (Sarid et al. 1986) were investigated by STM. Earlier studies of the optical properties and size distributions of  $\text{BiI}_3$  and related layered halides suggest that these colloidal microcrystallites grow as disks with a thickness of  $\cong 7 \text{ \AA}$  and lateral dimensions varying from  $\cong 12$  to  $\cong 90 \text{ \AA}$  depending on growth conditions, as shown in Figure 4.1 (Sandroff et al. 1986).

The structural building block of these materials consists of a layer of metal atoms sandwiched between hexagonally closed-packed layers of iodine; the thickness of this sandwich is about  $7 \text{ \AA}$ , suggesting that the colloidal particles grow to be just a single unit cell in thickness. The high degree of anisotropy seen in the growth of these clusters is consistent with the layered nature of the material in which strong chemical bonds exist within the I-Bi-I sandwich, while weak van der Waals forces are responsible for holding these units together. The layered-structure of  $\text{BiI}_3$  makes clusters of this material ideal candidates to be probed by STM since the tip can be scanned over the entire extent of the cluster without any interference from topographical defects.

Clusters of  $\text{BiI}_3$  were deposited by placing a drop of the colloidal suspensions on a graphite substrate and allowing the solvent to evaporate. This procedure made it difficult to locate isolated clusters, since the volume fraction of clusters in the suspension was only  $\cong 10^{-5}$ . In a typical scan we encountered large islands, at least  $10\text{-}100 \text{ \AA}$  in diameter, which could not be atomically resolved. Between these large islands, we would often be able to image the atomic structure of the

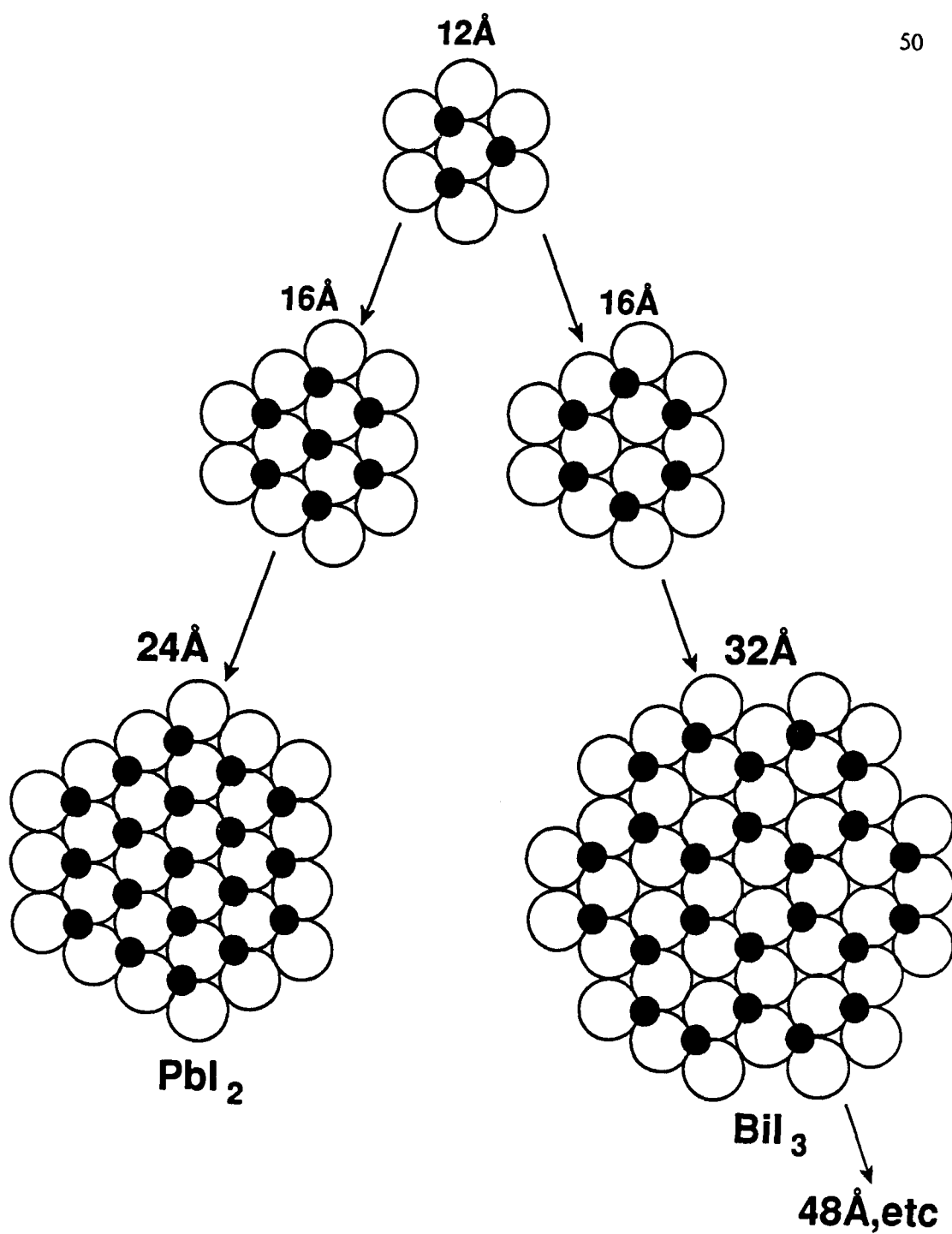


Figure 4.1 Predicted structure of layered  $\text{PbI}_2$  and  $\text{BiI}_3$  semiconductor clusters.

graphite substrate. After an extensive search, we were finally able to record an atomically resolved image of an isolated cluster on the graphite surface. A grey scale image of the cluster with the graphite surface in the background is shown in Figure 4.2.

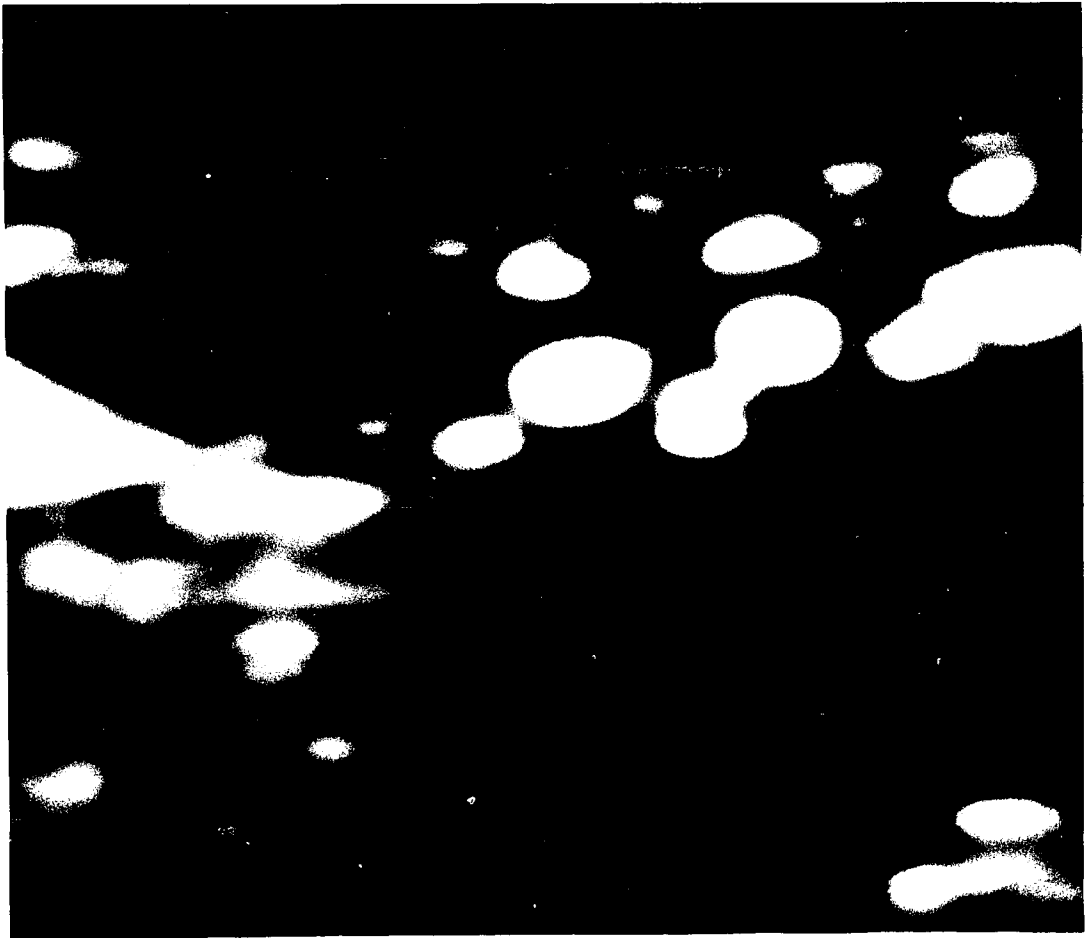
One can rule out the possibility that the cluster is an extension of the graphite surface since (a) it has a honeycomb structure, and (b) the "brightness" of the image of the cluster atoms is much higher than that of the surrounding graphite atoms. The reason that the background in the vicinity of the cluster does not show any features is due to the fact that in the constant height mode the average tip-to-sample distance is held constant. Consequently, in the presence of strong atomic features associated with "hills", the "valleys" give rise to only a small tunneling current and as such are not imaged.

The cluster imaged in Figure 4.2 consists of ten atoms arranged as two fused six-membered rings which have a distance of  $6.5 \pm 0.5 \text{ \AA}$  between ring centers with the possible presence of a partial third ring. Although we think that the image is due to the Bi atoms belonging to the  $\text{BiI}_3$  cluster, it is difficult to identify the exact composition of the cluster.

#### MoS<sub>2</sub> Clusters on Graphite

The next layered-structure semiconductor clusters investigated were MoS<sub>2</sub> clusters in colloidal suspensions. Since we had already made measurements on bulk MoS<sub>2</sub>, a unique opportunity existed to compare measurements of the bulk properties to those of the cluster. The structural building block of these materials, as in the bulk, consists of a layer of hexagonally open-packed molybdenum atoms

Figure 4.2 Grey scale image of a cluster on the surface of graphite obtained with a sample bias of 50 mV. The image represents an area of 25 Å X 20 Å.



sandwiched between hexagonally open-packed layers of sulfide atoms.

Clusters of  $\text{MoS}_2$  were deposited by placing a drop of the colloidal suspensions on a graphite substrate and allowing the solvent to evaporate. A hexagonal structure whose lattice spacing changed as the scan area was moved across the substrate was observed. The change in lattice spacing was so gradual that only one lattice spacing could be observed in the scan area at any given time. Also encountered were large islands 25 Å to 200 Å in length. Some of the islands could not be atomically resolved. However, after an extensive search, it was found that some islands, when "zoomed" in on, could be atomically resolved, and revealed a hexagonal symmetry that had an extremely small lattice spacing. Table 4.1 summarizes the range of lattice spacings observed. The lattice spacing of 3.4 Å could reflect Mo-Mo or the S-S (3.16 Å) spacing of bulk  $\text{MoS}_2$  or it could possibly reflect the Mo-S (3.66 Å) spacing of the cluster if it adhered to the graphite on its side (Wyckoff 1971). However, the larger spacings may be a result of the dragging or frictional force caused by the tip when it is too close to the surface. This observation is in agreement with the one observed during the experiment. The spacing always increased when we moved the scan area to the left side of the sample and decreased when the scan area was on the right side of the sample. If the sample had a large tilt in it so that the gap spacing was significantly less on the left side of the sample then the lattice spacing on the left side of the sample would be larger due to the larger frictional or dragging force of the tip. The smaller lattice spacing of 1.71 Å that was observed when we "zoomed" in on one of the large islands cannot be explained in this manner and is a real effect.

Table 4.1. Lattice spacings observed on MoS<sub>2</sub> clusters.

<u>Structure</u>	<u>Lattice Spacing</u>	<u>Standard Deviation in Spacing</u>
hexagonal	1.71 Å	0.118 Å
hexagonal	3.40 Å	0.375 Å
hexagonal	4.24 Å	0.442 Å
hexagonal	5.65 Å	0.557 Å
hexagonal	7.90 Å	1.070 Å

Figures 4.3 and 4.4 are three dimensional plots of the hexagonal structures with differing lattice spacings. Figure 4.5 shows a grey scale image of the island on which we "zoomed", and Figure 4.6 shows a grey scale image of the hexagonal structure that was observed on the island.

### Results and Conclusions

A fragment of an isolated semiconductor cluster deposited on graphite was atomically resolved by use of an STM. Hexagonal structures with different lattice spacings were observed when MoS<sub>2</sub> clusters were deposited on graphite and studied with an STM. The lattice spacings larger than the bulk MoS<sub>2</sub> spacing are most likely due to the dragging force between the tip and the sample. Also, an island of MoS<sub>2</sub> was atomically resolved and found to have a hexagonal structure with a lattice spacing of 1.71 Å. We found that the MoS<sub>2</sub> clusters possess the same hexagonal structure as the bulk, however, the lattice spacing tends to differ somewhat. By imaging many different size clusters with the STM, one can learn how a cluster evolves into the bulk material.

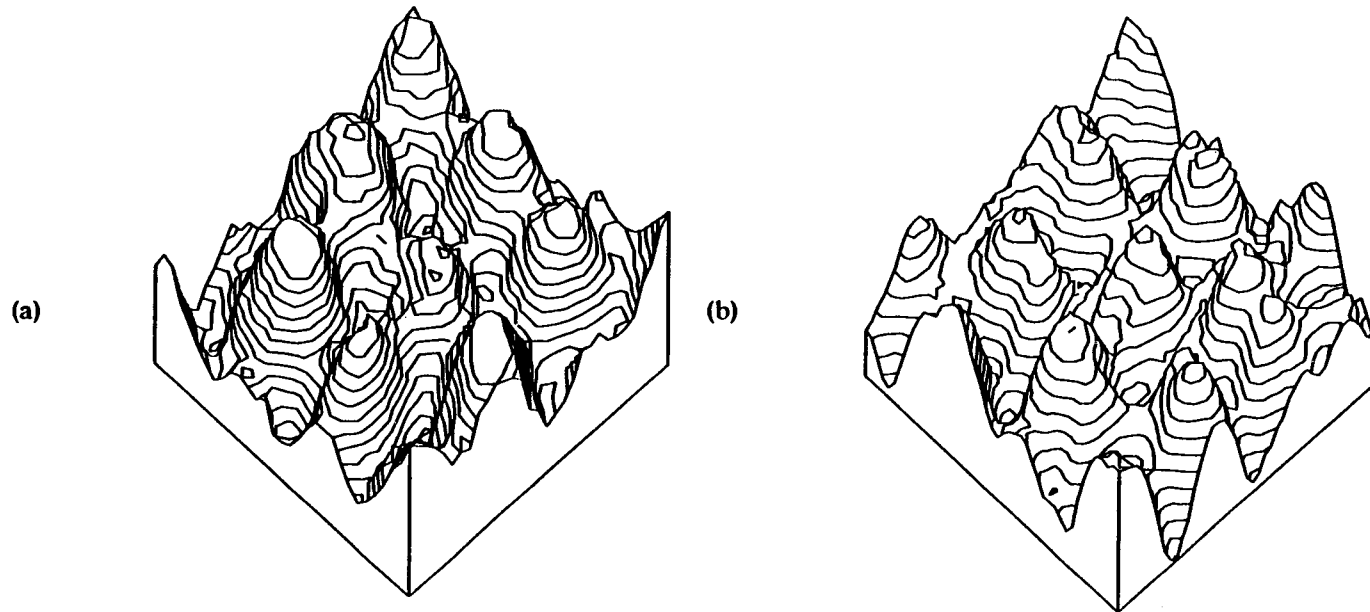


**Figure 4.3** Three dimensional presentations of the hexagonal structures observed when colloidal suspensions of MoS were deposited on a graphite substrate. The lattice spacings are (a) 3.4 Å and (b) 4.24 Å. The images represent areas of (a) 11.2 Å X 11.2 Å and (b) 9.2 Å X 9.2 Å and were obtained with a sample bias of -1 V.

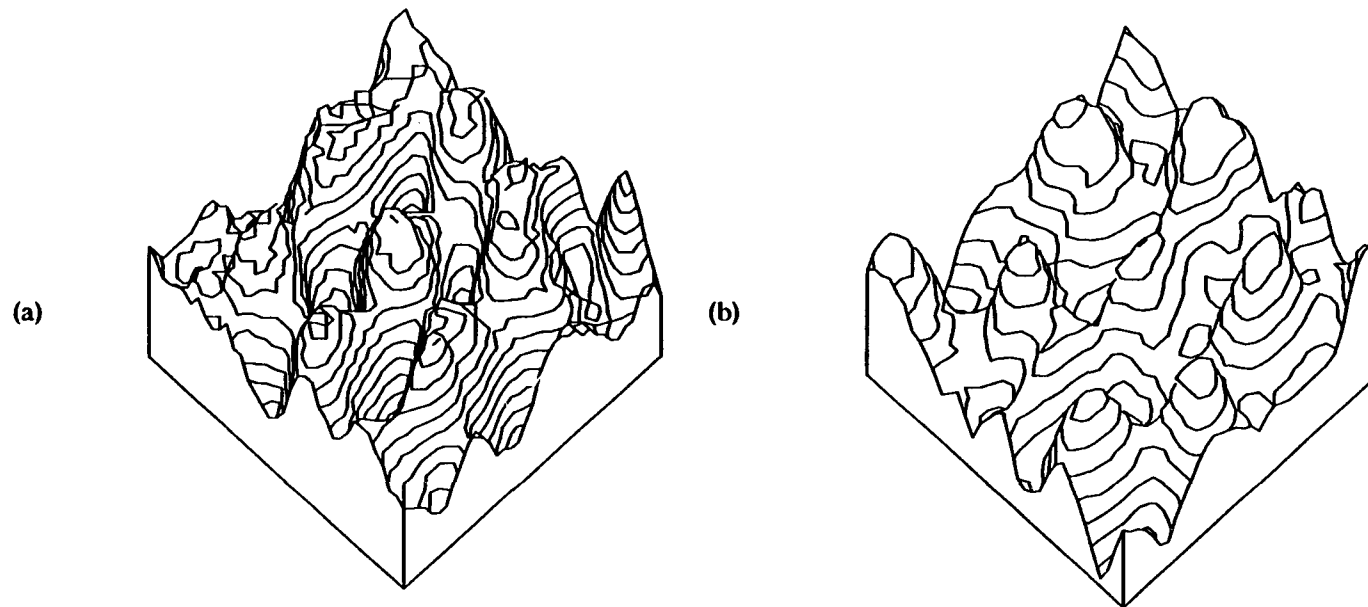


**Figure 4.4** Three dimensional presentations of the hexagonal structures observed when colloidal suspensions of MoS were deposited on a graphite substrate. The image lattice spacings are (a) 5.65 Å and (b) 7.9 Å. The images represent areas of (a) 16.3 Å X 16.3 Å and (b) 21 Å X 21 Å, and were obtained with a sample bias of 1 V.

Figure 4.5 Grey scale image of MoS<sub>2</sub> island on the surface of graphite. The image was obtained with a sample bias of -1 V and represents an area of 265 Å X 265 Å.

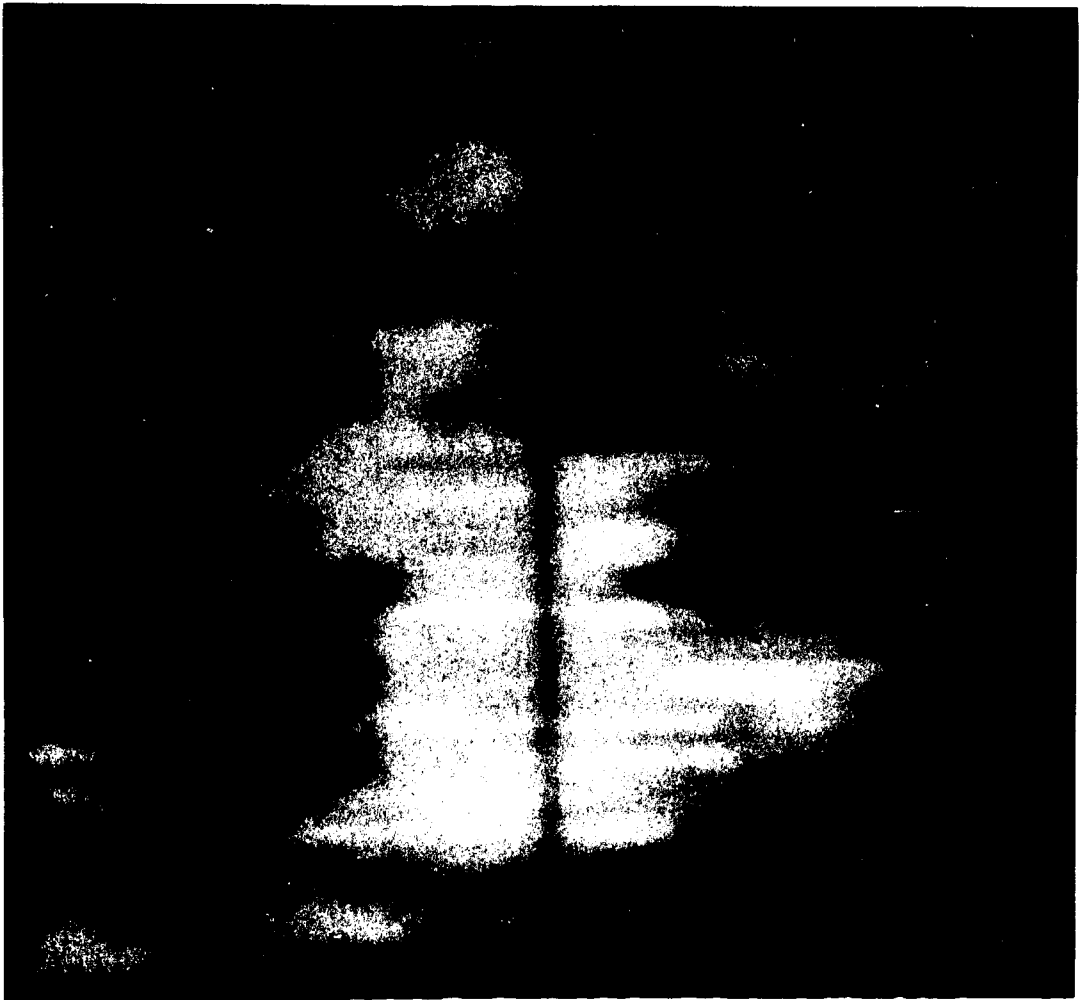
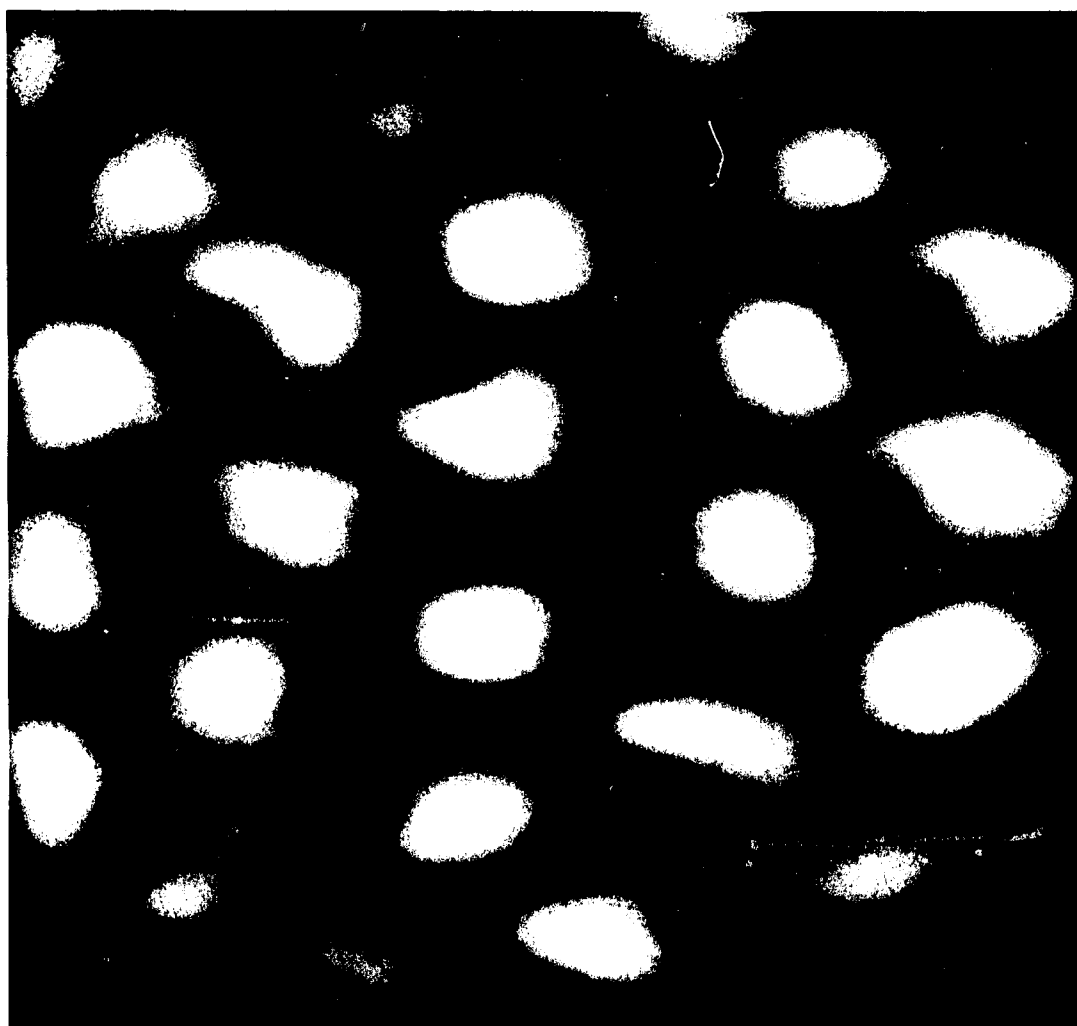


Figure 4.6 Atomically resolved grey scale image of a hexagonal structure observed on MoS<sub>2</sub> island. The image was obtained with a sample bias of -1 V and represents an area of 7.7 Å X 7.7 Å. The lattice spacing is approximately 1.7 Å.



## CHAPTER 5

### FUTURE STM RESEARCH

#### Quantum Confinement of Charge Carriers in Semiconductor Clusters

Quantum confinement of charge carriers inside a cluster takes place when the dimensions of the cluster becomes smaller than the de Broglie wavelength of the electron in the cluster. The confinement is manifested by a blue shift of the conduction and valence bands because small  $k$  vectors are not allowed anymore inside the cluster. This shift would not be seen in the bulk because it is a semi-infinite crystal and no quantum confinement effect exists. By comparing the observed density of states of the cluster with those of the bulk, one will be able to see if quantum confinement is present.

#### Improvements in Cluster Imaging

A key issue when imaging small isolated clusters on a substrate, is whether one probes the substrate or the cluster itself. Graphite can easily be atomically resolved, and due to interactions between the tip and the surface, the graphite images do not always possess the 2.45 Å lattice spacing, but rather spacings which are multiples of this. Therefore, one may be misled into thinking that a graphite image is actually an image of a cluster deposited on graphite. It is for this reason that we decided to use gold as a substrate for cluster imaging. Gold is extremely difficult to image on the atomic scale. Therefore, any atomic feature observed while imaging clusters on gold is most likely due to the cluster and not to the gold

substrate. One of the experiments which is currently being pursued, is imaging MoS<sub>2</sub> clusters on a gold substrate and comparing these results to those obtained on a graphite substrate. If the results agree we will feel confident that they represent the structure of the clusters deposited on the substrates.

### STM System Improvements

Currently, our STM system is being modified to reduce acoustic vibrations, reduce problems caused by thermal drift, and automate the system by providing switch control between the different modes of operation.

In air, acoustic vibrations can be quite large. One becomes especially sensitive to this type of vibration when working in the constant current mode. In this case, the STM picks up almost all the acoustic noise in the laboratory environment making it nearly impossible to work in the same room as the STM. An excellent way to isolate ones STM from acoustic noise is to place a pyrex bell jar over the STM. This also serves to overcome some of the problems with thermal drift since air currents can no longer flow through the STM. It is for these reasons that we are adding a pyrex bell jar to our STM system.

To help automate our system, we have added a switch control which will allow us to easily switch between our operating mode when we are collecting STM data, and our image processing and viewing modes. The switch control eliminates the need to manually change cables when one wants to image process new results or view previous results.

### Summary

By atomically resolving layered-structure semiconductors and measuring their density of states in the bulk and in the isolated cluster form, one can gain insight into how a cluster grows into the bulk material, how the symmetry or lattice parameters of a material change as a function of size, and how the size of a cluster modifies the linear optical response of the material. Using these methods, one can characterize materials both in bulk and in the isolated cluster form and gain insight into their size-dependent properties.

## REFERENCES

- Abraham, D. W., H. J. Mamin, E. Ganz, and J. Clarke, *IBM J. Res. & Dev.* **30**, 492 (1986a).
- Abraham, D. W., K. Sattler, E. Ganz, H. J. Mamin, R. E. Thomson and J. Clarke, *Appl. Phys. Lett.* **49B** 853 (1986b)
- Albrecht, T. R. and C. F. Quate, *J. Vac. Sci. & Tech. A* **6**, 271 (1988).
- Arlunya Image Processor, Princeton Electronics Products, North Brunswick, NJ 08902.
- Bando, H., H. Tokumoto, W. Mizutani, K. Watanabe, M. Okano, M. Ono, H. Muradami, S. Okayama, Y. Ono, S. Wayikama, F. Sakai, K. Endo and K. Kajimura, *Jpn. J. Appl. Phys.* **26**, L41 (1986).
- Baratoff, A., *Physica B* **127**, 143 (1984).
- Baratoff, A., G. Binnig, H. Fuchs, F. Salvan and E. Stoll, *Surf. Sci.* **168**, 734 (1986).
- Baro', A. M., R. Miranda, J. Alaman, N. Garcia, G. Binnig, H. Rohrer, Ch. Gerber, and J. L. Carrascosa, *Nature* **315**, 253 (1985).
- Binnig, G., H. Rohrer, Ch. Gerber, and E. Weibel, *Phys. Rev. Lett.* **49**, 57 (1982).
- Binnig, G., H. Rohrer, Ch. Gerber, and E. Weibel, *Phys. Rev. Lett.* **50**, 120 (1983).
- Binnig, G., H. Rohrer, Ch. Gerber, and E. Stoll, *Surf. Sci.* **144**, 321 (1984).
- Bryant, A., D. P. E. Smith and C. F. Quate, *Appl. Phys. Lett.* **48**, 832 (1986).

REFERENCES-Continued

- Coleman, R. V., B. Drake, P. K. Hansma, and G. Slough, *Phys. Rev. Lett.* **55**, 394 (1985).
- Elrod, S. A., A. L. de Lozanne, and C. F. Quate, *Appl. Phys. Lett.* **45**, 1240 (1984).
- Evans B. L., *Optical and Electrical Properties*, (D. Reidel Pub. Co., Boston, 1976).
- Feenstra, R. M., J. A. Stroscio and A. P. Fein, *Surf. Sci.* **181**, 295 (1987).
- Grasso, V., *Electronic structure and electronic transitions in layered materials*, (D. Reidel Pub. Co., Boston, 1986).
- Hansma, P. K. and J. Tersoff, *J. Appl. Physics*, **61**, R1 (1987).
- Hosler, W., R. J. Behm, E. Ritter, *IBM J. Res. Dev.* **30**, 403 (1986).
- Humbert, A., F. Salvan and C. Mouttet, *Surf. Sci.* **181**, 307 (1987).
- Lang, N. D., *Phys. Rev. Lett.* **56**, 1164 (1986a).
- Lang, N. D., *Phys. Rev. B* **34**, 5947 (1986b).
- Muralt, P. and D. W. Pohl, *Appl. Phys. Lett.* **48**, 515 (1986).
- Parkinson, A., *Surf. Sci.* **136**, 15 (1984).
- Peyghambarian, N. and G. R. Olbright, *Appl. Phys. Lett.* **48**, 1184 (1986).
- Rossetti, R., R. Hull, J. M. Gibson, and L. E. Brus, *J. Chem. Phys.* **82**, 552 (1984a).
- Rossetti, R., J. L. Ellison, J. M. Gibson, and L. E. Brus, *J. Chem. Phys.* **80**, 4464 (1984b).
- Sandroff, C. J., S. P. Kelty and D. M. Hwang, *J. Chem. Phys.* **85**, 5337 (1986)

## REFERENCES-Continued

- Sarid, D., B. K. Rhee, B. P. McGinnis and C. J. Sandroff, *Appl. Phys. Lett.* **49**, 1196 (1986).
- Sarid, D., T. Henson, L. S. Bell, C. J. Sandroff, *J. Vac. Sci. & Tech. A* **6**, 424 (1988a).
- Sarid, D., T. D. Henson, N. R. Armstrong, L. S. Bell, *Appl. Phys. Lett.* **52**, 2252 (1988b).
- Selloni, A., P. Carnevali, E. Tosatti and C. D. Chen, *Phys. Rev. B* **31**, 2602 (1985).
- Slough, C. G., W. W. McNairy, R. V. Coleman, B. Drake and P. K. Hansma, *Phys. Rev. B* **34**, 994 (1986).
- Sonnenfeld, R. and P. K. Hansma, *Science* **232**, 211 (1986a).
- Sonnenfeld, R. and B. C. Shardt, *Appl. Phys. Lett.* **49**, 1172 (1986b).
- Stickney, J. J., S. D. Rosace, B. C. Schardt, T. Solomon, A. T. Hubbard and B. A. Parkinson, *Surf. Sci.* **136**, 15 (1984).
- Stupian, G. W. and M. S. Leung, *Appl. Phys. Lett.* **51**, 1560 (1987).
- Tersoff, J. and D. R. Hamann, *Phys. Rev. B* **31**, 805 (1985).
- Tersoff, J. and D. R. Hamann, *Phys. Rev. Lett.* **50**, 1998 (1983).
- Tokumoto, H. and H. Bando, *J. Vac. Sci. Tech. A* **5**, 1090 (1987).
- Tributsch, H., *Structure and Bonding* **49**, 128 (1982).
- Tromp, R. M., R. J. Hamers and J. E. Demuth, *Science* **234**, 304 (1986).
- Tunneling Microscope Company, P.O. Box 1270, Menlo Park, CA 94026.
- Weller, H., A. Fojtik, and H. Henglein, *Chem. Phys. Lett.* **117**, 485 (1985).

REFERENCES-Continued

- Weimer, M., J. Kramar, C. Bai, and J. D. Baldeschwieler, *J. Vac. Sci. & Tech. A* **6**, 336 (1988).
- Wieting, T. J. and M. Schluter, *Electrons and phonons in Layered Crystal Structures*, (D. Reidez Pub. Co., Holland 1979).
- Wyckoff, R. W. G., *Crystal Structures*, (Interscience Pub., New York 1971).
- Young, R., J. Ward, and F. Scire, *Rev. Sci. Inst.* **43**, 999 (1972).